



Photometric Observations of Supernova 2013cq Associated with GRB 130427A

R. L. Becerra¹, A. M. Watson¹, W. H. Lee¹, N. Fraija¹, N. R. Butler², J. S. Bloom³, J. I. Capone⁴, A. Cucchiara⁵, J. A. de Diego¹, O. D. Fox⁶, N. Gehrels⁷, L. N. Georgiev¹, J. J. González¹, A. S. Kutyrev⁷, O. M. Littlejohns², J. X. Prochaska⁸, E. Ramirez-Ruiz⁸, M. G. Richer⁹, C. G. Román-Zúñiga⁹, V. L. Toy⁴, and E. Troja^{4,7}

¹ Instituto de Astronomía, Universidad Nacional Autónoma de México, Apartado Postal 70-264, 04510 México, D. F., México

² School of Earth and Space Exploration, Arizona State University, Tempe, AZ 85287, USA

³ Department of Astronomy, University of California, Berkeley, CA 94720-3411, USA

⁴ Department of Astronomy, University of Maryland, College Park, MD 20742, USA

⁵ NASA Postdoctoral Program Fellow, Goddard Space Flight Center, Greenbelt, MD 20771, USA

⁶ Space Telescope Science Institute, 3700 San Martin Drive, Baltimore, MD 21218, USA

⁷ NASA, Goddard Space Flight Center, Greenbelt, MD 20771, USA

⁸ Department of Astronomy and Astrophysics, UCO/Lick Observatory, University of California, 1156 High Street, Santa Cruz, CA 95064, USA

⁹ Instituto de Astronomía, Universidad Nacional Autónoma de México, Apartado Postal 106, 22800 Ensenada, Baja California, México

Received 2016 April 25; revised 2017 February 13; accepted 2017 February 14; published 2017 March 9

Abstract

We observed the afterglow of GRB 130427A with the Reionization and Transients Infrared Camera (RATIR) instrument on the 1.5 m Harold L. Johnson telescope of the Observatorio Astronómico Nacional in Sierra San Pedro Martir. Our homogenous *griZ* photometry extends from the night of the burst to three years later. We fit a model for the afterglow. There is a significant positive residual that matches the behavior of SN 1998bw in the *griZ* filters; we suggest that this is a photometric signature of the supernova SN 2013cq associated with the Gamma-ray burst. The peak absolute magnitude of the supernova is $M_r = -18.43 \pm 0.11$.

Key words: gamma-ray burst: individual (GRB 130427A) – supernovae: individual (2013cq)

1. Introduction

Gamma-ray bursts (GRBs) are the most energetic events in the universe and are produced at cosmological distances. They can be classified according to their duration T_{90} , the time interval in the observer's frame over which 90% of the total background-subtracted counts are observed (Koshut et al. 1995). This parameter has long pointed to a bi-modal distribution (Kouveliotou et al. 1993).

Long GRBs ($T_{90} > 2$ s) are today thought to be the result of the core-collapse of a star (Woosley 1993; MacFadyen & Woosley 1999; Hjorth & Bloom 2012) with an initial mass of more than $10 M_\odot$ (see Woosley & Bloom 2006, for a review), while short GRBs ($T_{90} < 2$ s) are thought to be the result of mergers between two compact objects (Lattimer & Schramm 1976; Eichler et al. 1989; Paczynski 1989, 1991; Narayan et al. 1992) like black holes or neutron stars (see Lee & Ramirez-Ruiz 2007; Nakar 2007, for reviews).

Woosley (1993) specifically proposed a way in which the core-collapse of massive stars could lead to a long GRB, and thus be possibly associated with a supernova (SN; Woosley & Bloom 2006; Modjaz 2011; Bersier 2012; Hjorth 2013). In this scenario, the optical emission from the SN would appear a few days after the GRB, when the ejecta becomes optically thin. This leads to two ways to identify the presence of an SN associated with a GRB: (1) by the appearance of the broad spectral lines that are characteristic of SN a few days after the burst; and (2) through a rebrightening in the light curve of the GRB after a few days due to the broadband emission of the SN. The identification of a SN associated with GRB 980425 (Galama et al. 1998) showed that at least some GRBs are truly linked to the core-collapse of massive stars.

Subsequently, other SNe have also been associated with long GRBs. Confirmed spectroscopic cases are listed in Table 1. Most or perhaps all of these SNe are Type Ic. Usually, the hosts of GRB-SNe are blue, star-forming galaxies (Fynbo et al. 2000;

Foley et al. 2006; Fruchter et al. 2006; Hammer et al. 2006; Niino 2013) and the events occur within a low-metallicity environment (Modjaz et al. 2008).

Simply taking into account the rates of SNe and GRBs, however, it is apparent that not all core-collapse SNe produce long GRBs, and special conditions are required in order to successfully power a burst. These probably involve rotation, magnetic fields, chemical composition, binarity, or a combination of the above, and are not yet fully resolved. Thus, precise observations of a significant sample of GRBs associated with SNe are fundamental in order to determine the evolutionary pathways that can lead to such a link. Given that the current sample is extremely limited, studying single events like SN 2013cq associated with GRB 130427A in great detail offers the opportunity to provide unique additional insights and to eventually lead the way to a statistically significant sample, and this is the main motivation for the present paper.

GRB 130427A is one of the brightest GRBs of the last few years, and had $E_{\gamma,\text{iso}} = 1.40 \times 10^{54}$ erg in total isotropic energy release (Ackermann et al. 2014) and $E_{\gamma,\text{peak}} = 1028 \pm 8$ keV (Maselli et al. 2014). It was detected at high energies by several satellite instruments and lead to a flurry of ground-based observations. In total, there have been 91 GCN Circulars related to GRB 130427A. Its redshift was measured to be $z = 0.34$ (Levan et al. 2013). RAPTOR (the Rapid Telescope for Optical Response) observed a bright optical flash with a magnitude of 7.03 ± 0.03 in the time interval from 9.31 to 19.31 s after the GBM trigger (Vestrand et al. 2014). The bright optical flash at early times was modeled with synchrotron emission from reverse shocks (Vestrand et al. 2014; Fraija et al. 2016). Perley et al. (2014) show multi-wavelength optical/infrared photometry of the afterglow of GRB 130427A, and explain the afterglow through synchrotron radiation and suggest a massive-star progenitor. Spectroscopy with the 10.4 m GTC telescope reported by Xu et al.

Table 1
GRBs with Associated SN

GRB	SN	SN Type	z	Evidence ^a	References
GRB 980425	SN 1998bw	Ic	0.0085	A	1
GRB 011121	SN 2001ke	IIn?/Ic?	0.362	B	2, 3, 4
GRB 021211	SN 2002lt	Ic	1.006	B	5
GRB 030329	SN 2003dh	Ic	0.1687	A	6, 7
GRB 031203	SN 2003lw	Ic	0.105	A	8, 9, 10
GRB 050525A	SN 2005nc	Ic	0.606	B	11
GRB 060218	SN 2006aj	Ic	0.0335	A	12, 13, 14, 15, 16
GRB 081007	SN 2008hw	Ic	0.530	B	17, 18, 19
GRB 091127	SN 2009nz	Ic	0.49	A	20, 21
GRB 100316D	SN 2010bh	Ic	0.059	A	22, 23, 24, 25, 26
GRB 120422A	SN 2012bz	Ic	0.283	A	27, 28
GRB 130427A	SN 2013cq	Ic	0.34	A	29, 30, 31
GRB 130702A	SN 2013dx	Ic	0.145	A	32, 33
GRB 140606B	iPTF14bfu	Ic	0.384	A	34

Notes.

^a Evidence for the GRB-SN association, according to the authors, with A meaning strong spectroscopic evidence and B meaning a clear light curve bump together with some spectroscopic evidence resembling a SN.

^b SN 2001ke has no clear spectroscopic classification. Garnavich et al. (2003) suggest that it is a Type IIn but Bloom et al. (2002) claim it is indeed consistent with a 1998bw-like Type Ic.

References. (1) Galama et al. (1998), (2) Bloom et al. (2002), (3) Garnavich et al. (2003), (4) Greiner et al. (2003), (5) Della Valle et al. (2003), (6) Stanek et al. (2003), (7) Matheson et al. (2003), (8) Malesani et al. (2004), (9) Gal-Yam et al. (2004), (10) Thomsen et al. (2004), (11) Della Valle et al. (2006), (12) Campana et al. (2006), (13) Modjaz et al. (2008), (14) Mirabal et al. (2006), (15) Ferrero et al. (2006), (16) Pian et al. (2006), (17) Berger et al. (2008), (18) Della Valle et al. (2008), (19) Soderberg et al. (2008), (20) Cobb et al. (2010), (21) Berger et al. (2011), (22) Starling et al. (2011), (23) Bufano et al. (2012), (24) Olivares et al. (2012), (25) Cano et al. (2011), (26) Chornock et al. (2010), (27) Melandri et al. (2012), (28) Schulze et al. (2014), (29) de Ugarte Postigo et al. (2013), (30) Xu et al. (2013a), (31) This work; (32) Toy et al. (2015), (33) D'Elia et al. (2015), and (34) Cano et al. (2015).

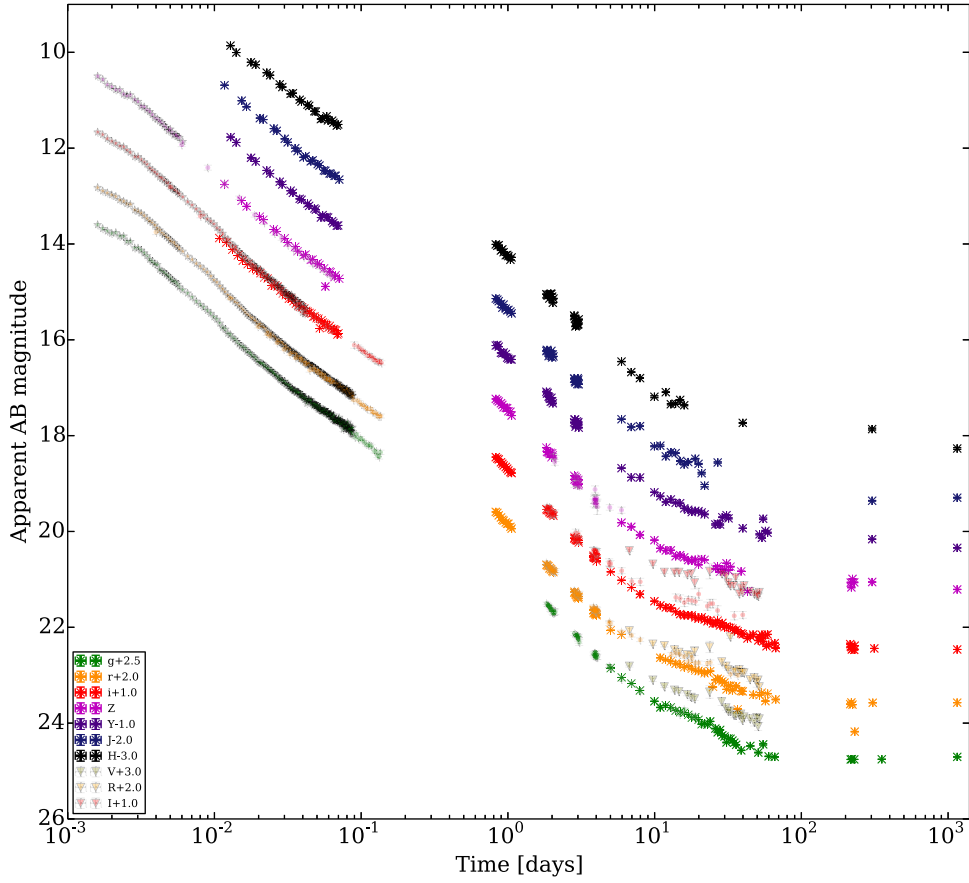


Figure 1. *grizY JH* light curves for GRB 130427A from RATIR (lines), RAPTOR (Maselli et al. 2014; stars), Palomar P60 (Perley et al. 2014; points) and VLT (Melandri et al. 2014; triangles). The RATIR photometry shown here is our aperture photometry of the afterglow and host galaxy.

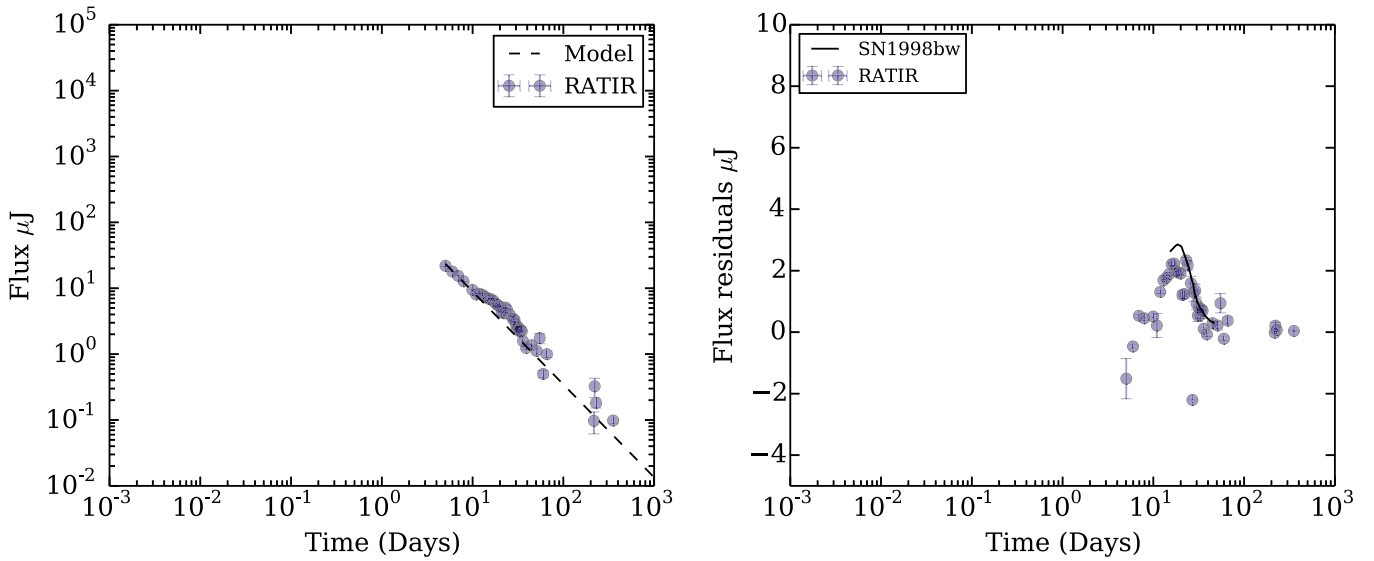


Figure 2. Left: the host-subtracted data (points) and power-law model (dashed line) in the g filter of RATIR (points). Right: flux density residuals in g (points) and the flux density of SN 1998bw in U shifted to $z = 0.34$ (continuous line).

Table 2
Host Galaxy Magnitudes for GRB 130427A

Filter	m_{RATIR}	Exposure (hr)	m_{SDSS}
g	22.20 ± 0.04	10.6	22.14 ± 0.12
r	21.57 ± 0.04	6.5	21.41 ± 0.10
i	21.46 ± 0.03	17.8	21.53 ± 0.23
Z	21.29 ± 0.05	8.3	...
Y	21.34 ± 0.07	8.2	...
J	21.30 ± 0.09	8.0	...
H	21.27 ± 0.13	7.9	...

Table 3
Fit Parameters

Parameter	Band	Value
α_E	...	0.97 ± 0.04
A_E	i	$303 \pm 28 \mu\text{Jy}$
A_E	Z	$348 \pm 38 \mu\text{Jy}$
A_E	Y	$373 \pm 38 \mu\text{Jy}$
A_E	J	$364 \pm 37 \mu\text{Jy}$
A_E	H	$373 \pm 27 \mu\text{Jy}$
α_L	...	1.41 ± 0.04
A_L	g	$228 \pm 12 \mu\text{Jy}$
A_L	r	$268 \pm 10 \mu\text{Jy}$
A_L	i	$315 \pm 20 \mu\text{Jy}$
A_L	Z	$388 \pm 37 \mu\text{Jy}$
A_L	Y	$436 \pm 18 \mu\text{Jy}$
A_L	J	$426 \pm 11 \mu\text{Jy}$
A_L	H	$489 \pm 116 \mu\text{Jy}$

(2013a) showed a broad-lined Ic SN 2013cq associated with GRB 130427A.

This paper presents a detailed set of calibrated and uniform photometry of the bright GRB 130427A with the Reionization and Transients Infrared Camera (RATIR) instrument in the $griZYJH$ filters. The major advantages of our work compared to earlier papers (Xu et al. 2013a; Melandri et al. 2014; Perley et al. 2014) is that our photometry is generally deeper, has

better temporal sampling, and we subtract the host galaxy using deep late-epoch images. Furthermore, our data were all obtained with the same instrument, using the same observing strategy, and were all processed in the same way. This means that our data are naturally homogeneous. The paper is organized as follows: in Section 2 we present the observations; in Section 3 we fit the data using segments of a power-law according to the fireball model; in Section 4 we search for the signature of SN 2013cq in the difference between the host-subtracted measurements and the power-law afterglow model; and in Section 5 we discuss the results and summarize our conclusions.

2. Observations

2.1. Fermi and Swift

The Gamma-Ray Burst Monitor (GBM) instrument on the *Fermi* satellite triggered on GRB 130427A at 07:47:06.42 UTC on 2013 April 27 (von Kienlin 2013). Subsequently, the Burst Alert Telescope (BAT) on the *Swift* satellite triggered on the GRB at 07:47:57.51 UTC (Maselli et al. 2014). The duration measured with BAT was $T_{90} = 163$ s (Barthelmy et al. 2013), making GRB 130427A a long GRB.

2.2. Ratir

The RATIR is a four-channel simultaneous optical and near-infrared imager mounted on the 1.5 m Harold L. Johnson Telescope at the Observatorio Astronómico Nacional in Sierra San Pedro Martir in Baja California, Mexico. RATIR responds autonomously to GRB triggers from the *Swift* satellite and obtains simultaneous photometry in $riZJ$ or $riYZH$ (Butler et al. 2012; Watson et al. 2012; Littlejohns et al. 2015). In manually programmed follow-up observations, the g filter can be substituted for r .

RATIR began to observe the field of GRB 130427A 15.5 minutes after the BAT trigger, and continued to observe it intensively over the subsequent weeks. On the first night, the r detector failed, so we only have data in $iZYJH$. On subsequent nights, we have data in $riZYJH$. After one week, we began to

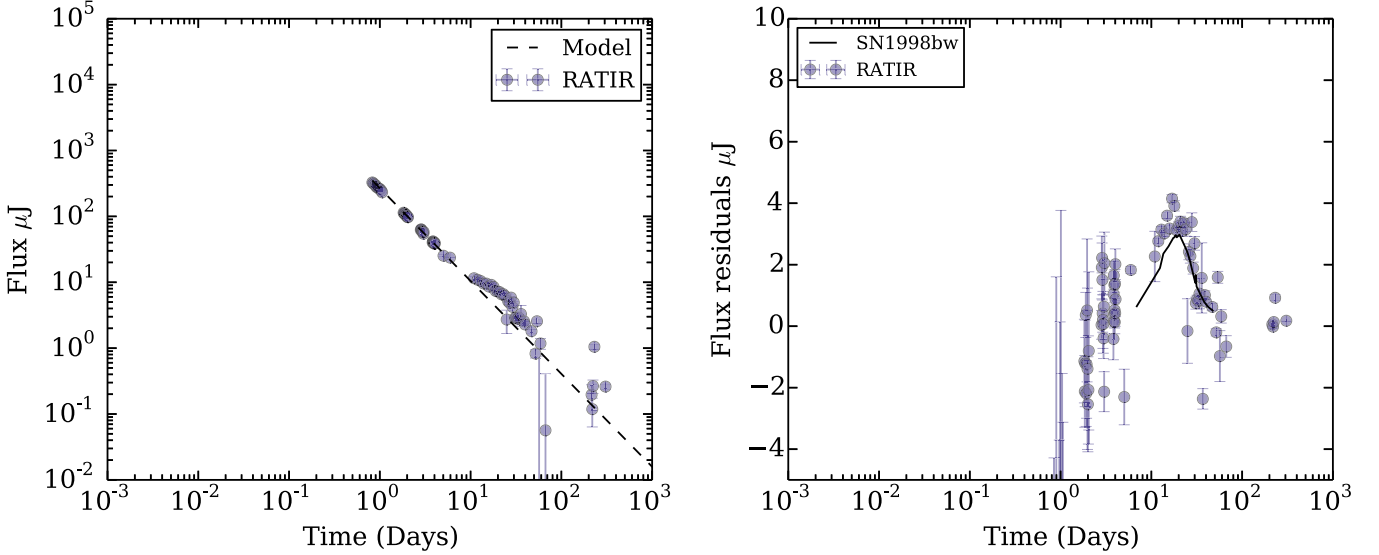


Figure 3. Left: the host-subtracted data (points) and power-law model (dashed line) in the r filter of RATIR (points). Right: flux density residuals in r (points) and the flux density of SN 1998bw in B shifted to $z = 0.34$ (continuous line).

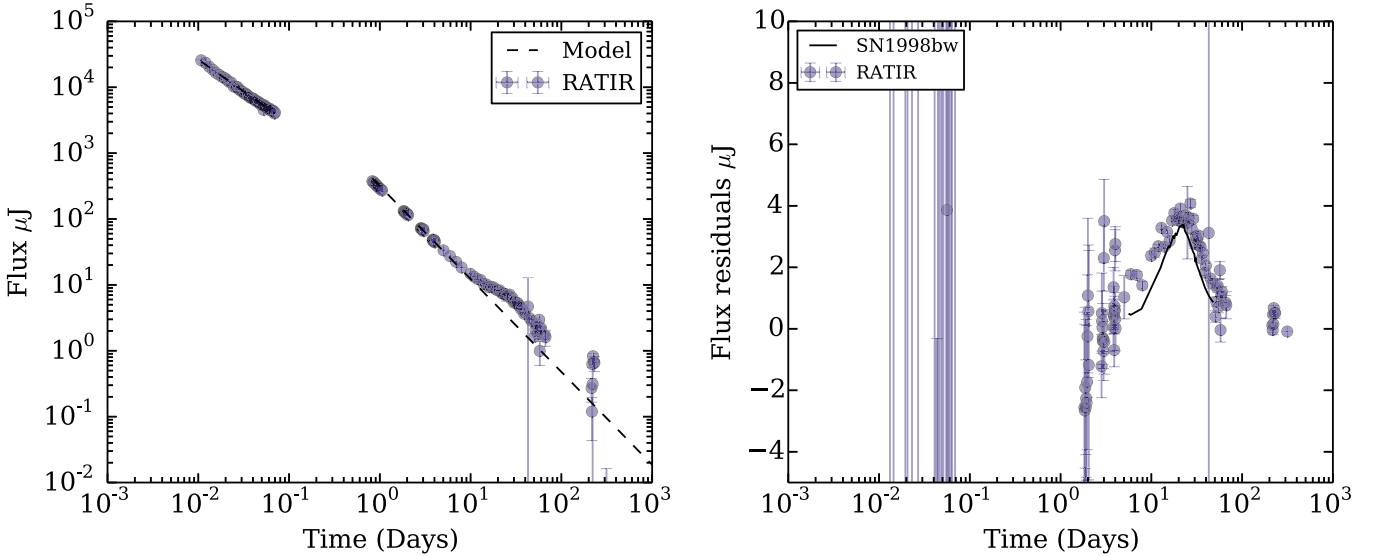


Figure 4. Left: the host-subtracted data (points) and power-law model (dashed line) in the i filter of RATIR (points). Right: flux density residuals in i (points) and the flux density of SN 1998bw in V shifted to $z = 0.34$ (continuous line).

observe in g as well. We reobserved the field on several nights in 2014 and 2016 mainly to place constraints on the host galaxy.

Our reduction pipeline performs bias subtraction and flat-field correction, followed by astrometric calibration using the astrometry.net software (Lang et al. 2010), iterative sky-subtraction, coaddition using SWARP, and source detection using SExtractor (Littlejohns et al. 2015). We calibrate against SDSS and 2MASS (Littlejohns et al. 2015). The systematic calibration error is about 1%.

The individual exposures were 80 s in gri and 67 s in $ZYJH$ filters (with the infrared exposures being shorter because of their longer read-out overhead). On the first night, we consider the exposures individually. For the second to the fifth night, we combined sets of 16 exposures taken over about 30 minutes to improve the signal-to-noise ratio. For the remaining nights in

2013, we combined all of the exposures for each night, for 2014, we combined several nights, and for 2016, we combined all of the exposures. The image quality in the final images was typically 2 arcsec FWHM.

We obtained aperture photometry using a 3 arcsec diameter aperture. Table 6 gives our aperture photometry. For each image it gives the start and end time, t_0 and t_f , the total exposure time t_e , the magnitude, the 1σ total uncertainty (including both statistical and systematic contributions), and the filter. These magnitudes are not corrected for Galactic extinction.

We also obtained point-spread function (PSF)-fitting photometry of the afterglow and supernova in our 2013 and 2014 images after subtracting the host galaxy using our 2016 image. For each image, we estimated the PSF by co-aligning and summing images of stars (as categorized by the SDSS) within

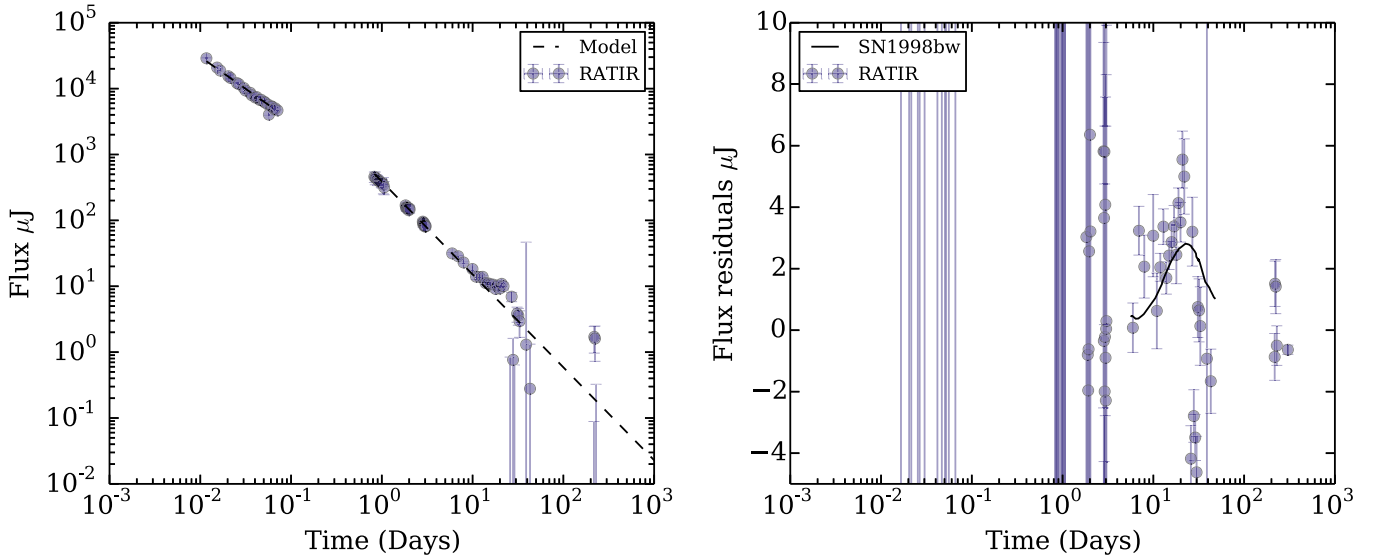


Figure 5. Left: the host-subtracted data (points) and power-law model (dashed line) in the Z filter of RATIR (points). Right: Flux density residuals in Z (points) and the flux density of SN 1998bw in R shifted to $z = 0.34$ (continuous line).

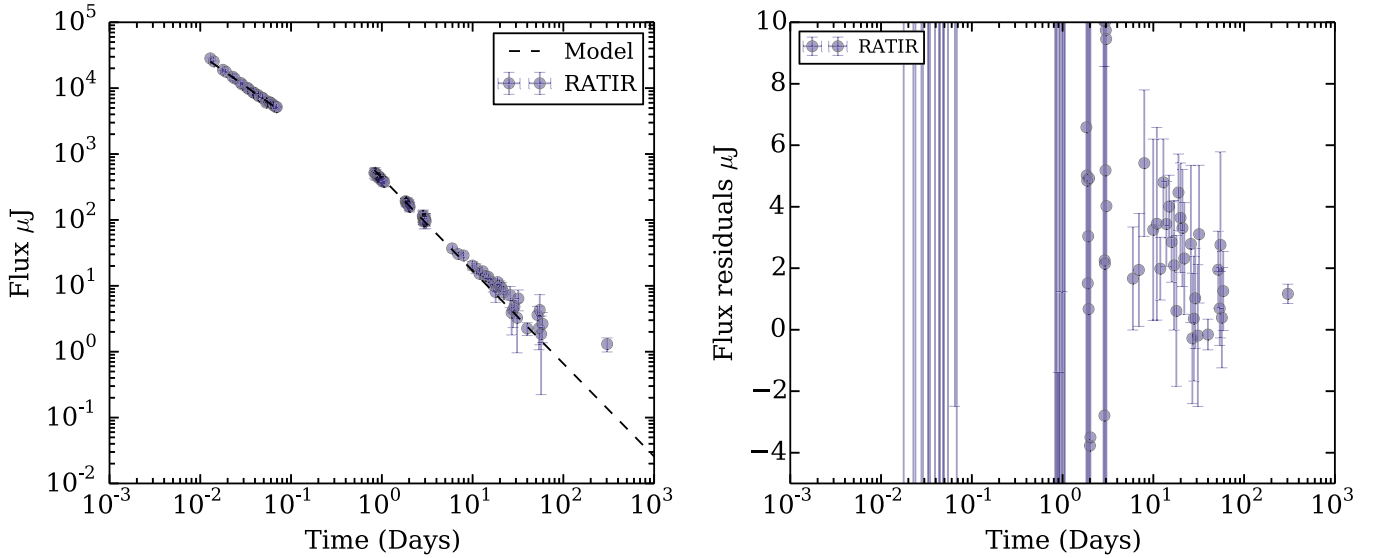


Figure 6. Left: the host-subtracted data (points) power-law model (dashed line) in the Y filter of RATIR. Right: flux density residuals in Y (points).

3 arcmin of the GRB. We subtracted the 2016 image from the earlier images using HOTPANTS (Becker 2015) and fitted the PSF to the residual. Even though our image quality is typically 2 arcsec FWHM, we cannot reliably perform PSF-fitting on the unsubtracted images because the galaxy is offset about 0.8 arcsec to the southeast of the afterglow (Levan et al. 2014). Table 6 also gives our PSF-fitting photometry. The main advantage of PSF-fitting is that the statistical uncertainties are reduced typically by about 20%. Figure 1 shows the RATIR optical and near-infrared light curves.

3. Models

The standard fireball model for GRBs (Kumar & Zhang 2015) distinguishes two stages: the *prompt emission* and the *afterglow*. The prompt emission is simultaneous with emission in gamma-rays and is produced by internal shocks in

the jet driven by the central engine. The afterglow is produced by the external shock between the jet and the circumstellar environment (e.g., Kumar & Piran 2000; Fraija 2015).

The emission region of the radiation determines the form and behavior of the spectrum and light curve for a GRB (e.g., Fraija et al. 2016), and can be different for each filter. Optical radiation has three possible origins: internal shocks in the jet, the forward external shock, and the reverse external shock (Sari & Piran 1999).

The afterglow phase can be explained by assuming a power-law energy distribution of shocked relativistic electrons, $N(E) \propto E^{-p}$, which leads to the observed flux being a series of power-law segments as a function of time t and frequency ν as $F_\nu^{\text{syn}} \propto t^{-\alpha} \nu^{-\beta}$ (Sari & Piran 1998).

RATIR began to observe after the end of the prompt emission, so we only have photometry for the afterglow. We divided these

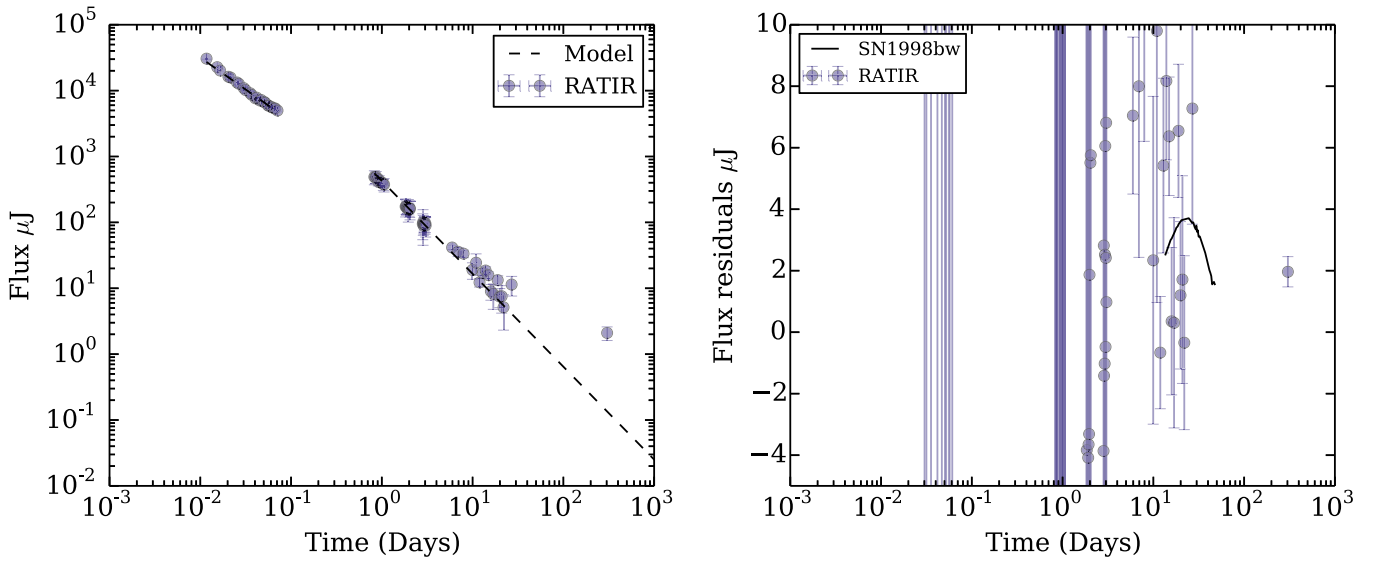


Figure 7. Left: the host-subtracted data (points) and power-law model (dashed line) in the J filter of RATIR. Right: flux density residuals in J (points) and the flux density of SN 1998bw in I shifted to $z = 0.34$ (continuous line).

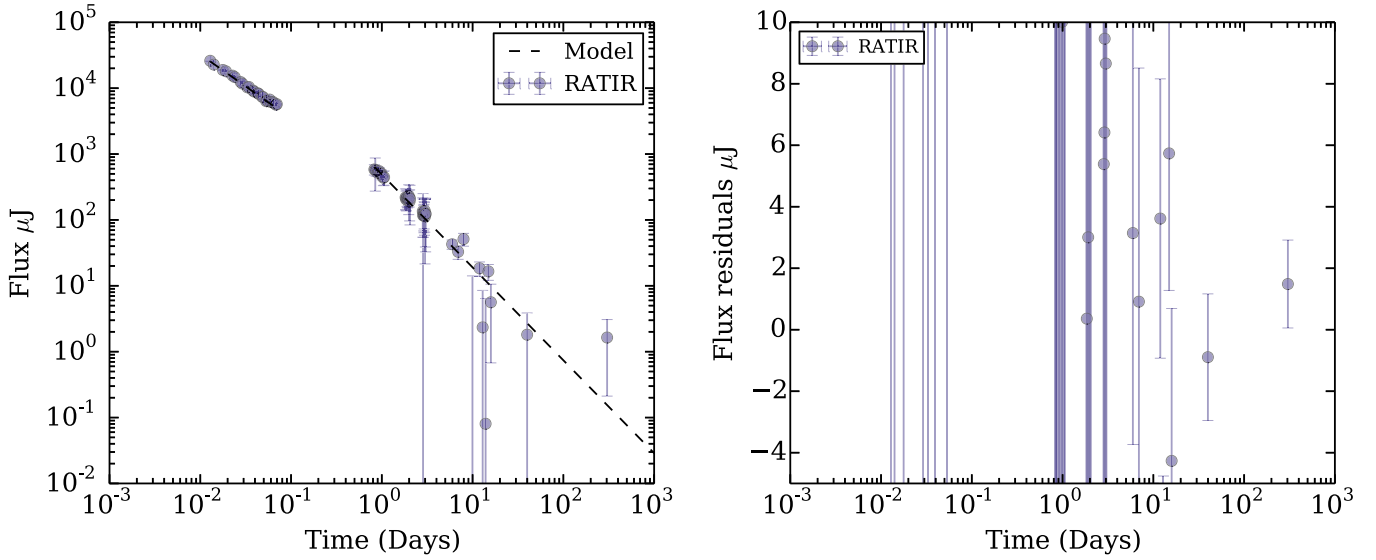


Figure 8. Left: the host-subtracted data (points) and power-law model (dashed line) in the H filter of RATIR. Right: flux density residuals in H (points).

Table 4

Correspondence between RATIR Filters at $z = 0.34$ and Johnson–Cousins Filters at $z \approx 0$

Filter	λ (nm) $z = 0$	λ (nm) $z = 0.34$	Filter	λ (nm) $z = 0$
g	470	351	U	360
r	618	461	B	440
i	760	567	V	550
Z	878	655	R	640
Y	1020	761	I	759
J	1250	932
H	1635	1220	J	1260

data into two epochs: the *early* afterglow for time $t < 0.1$ days (the first night) and the *late* afterglow for the $t > 0.7$ day (the second and subsequent nights). This division was guided by the

analysis of Perley et al. (2014), who reported a change in the slope of the light curve at $t = 0.7$ days. We have no data between $t = 0.1$ and $t = 0.7$ days.

3.1. Host Galaxy

Vonova et al. (2013) suggested that SDSS DR12 galaxy object 1237667431180861948 was the host galaxy of the GRB. This was subsequently confirmed by the close agreement in redshift between absorption lines in the GRB spectrum (Flores et al. 2013; Levan et al. 2013; Xu et al. 2013b) and emission lines from the galaxy (Xu et al. 2013a).

Levan et al. (2014) obtained *HST* images of the afterglow and host galaxy. They suggested that the host is a moderately star-forming, possibly interacting, disk galaxy, and the GRB occurred about 0.8 arcsec (4 kpc) from the nucleus.

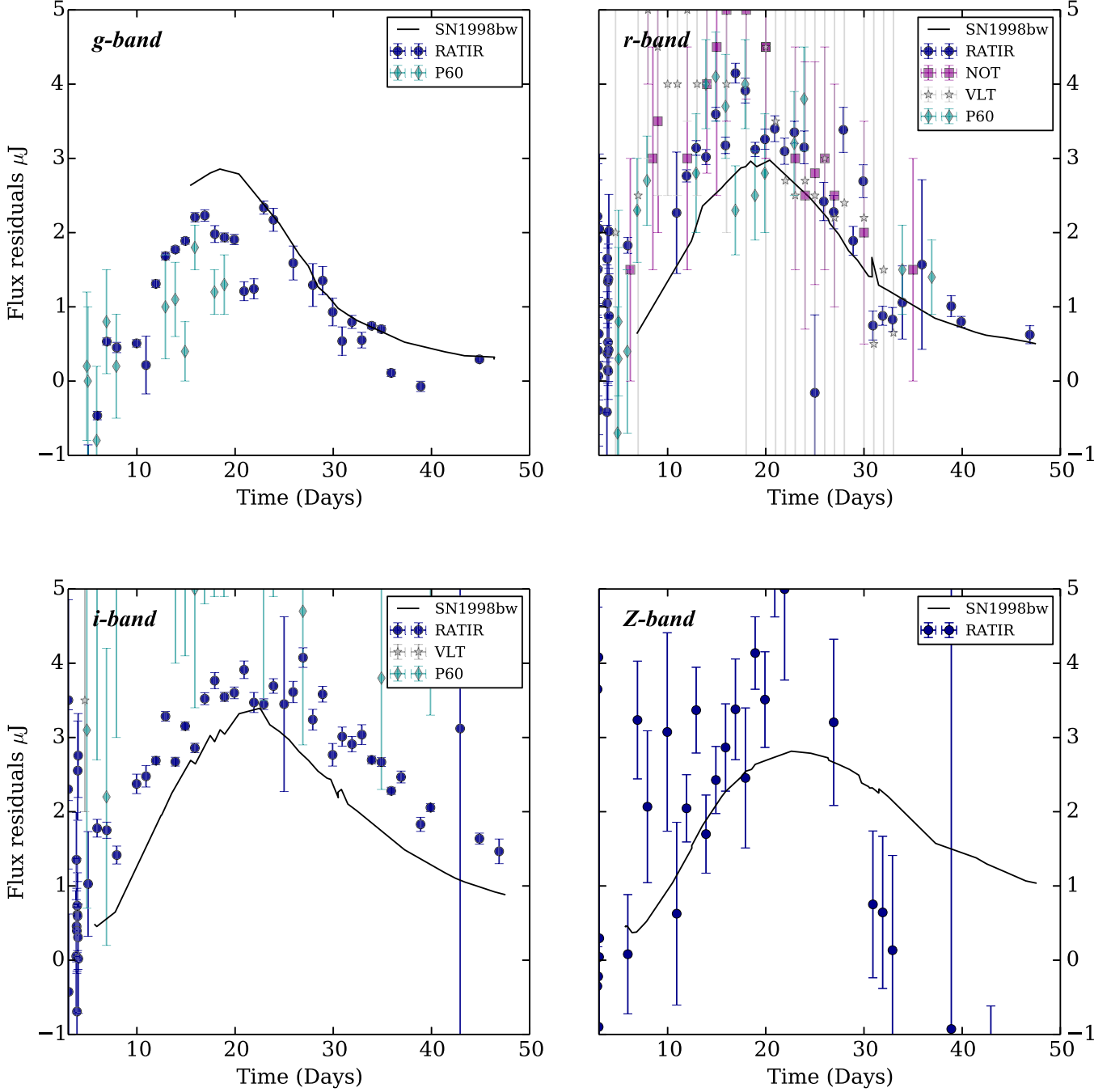


Figure 9. Light curves of SN 2013cq associated with GRB 130427A in the *griZ* bands. RATIR from this work (points), P60 from Perley et al. (2014; diamonds), NOT from Xu et al. (2013a; squares), and VLT from Melandri et al. (2014; stars). The line shows that the light curves for SN 1998bw are shifted to $z = 0.34$.

Table 2 reports our RATIR *griZYJH* aperture magnitudes from 2016 and magnitudes from the SDSS DR12 image using the same apertures and calibrating stars. The magnitudes from our image are consistent with the magnitudes from the SDSS image, but have lower uncertainties.

We can estimate the rest-frame $g - i$ color and M_i magnitude from our observed $r - Y$ color and Y magnitude (see Table 4 for the correspondence between rest-frame and observed bands) assuming a Λ CDM model with a $H_0 = 67.8 \text{ km Mpc}^{-1} \text{ s}^{-1}$ (Planck Collaboration et al. 2014). We obtain a rest-frame $g - i = 0.23 \pm 0.08$ and a rest-frame $M_i = -19.91 \pm 0.07$. These properties place it among the most extremely blue galaxies in the $z \approx 0$ sample of Gavazzi et al. (2010).

3.2. Early Afterglow ($t < 0.7$ days)

To characterize the early afterglow data ($t < 0.7$ days), we used the *iZYJH* aperture photometry from Table 6, as the contribution of the host galaxy can be neglected at early times. We fitted the flux densities with a power-law model $F = A_E t^{-\alpha_E}$, in which F is the flux density in the filter, A_E is a constant, t is the time since the BAT trigger (in days), and α_E is the temporal index, assumed to be the same for all filters. The model has six free parameters: the five values of A_E and the one value of the index α_E .

We minimized the value of χ^2 to find the best-fit parameters. The final fit has a $\chi^2/n = 1.64$ with $n = 100$ degrees of freedom. The best-fit parameters are given in Table 3. The

Table 5
Peak Flux Densities and Absolute Magnitudes for SN 2013cq
and SN 1998bw Shifted to $z = 0.34$

Band	SN 2013cq		SN 1998bw at $z = 0.34$	
	F_ν (μJy)	M	F_ν (μJy)	M
g	$+1.77 \pm 0.12$	-17.97 ± 0.07	2.58 ± 0.07	-18.38 ± 0.03
r	$+2.70 \pm 0.28$	-18.43 ± 0.11	2.82 ± 0.08	-18.48 ± 0.03
i	$+3.59 \pm 0.23$	-18.74 ± 0.07	3.15 ± 0.09	-18.60 ± 0.03
Z	$+2.80 \pm 0.87$	-18.47 ± 0.33	2.70 ± 0.07	-18.43 ± 0.03
Y	$+3.30 \pm 1.86$	-18.65 ± 0.61
J	$+2.28 \pm 2.69$	-18.24 ± 0.28	3.57 ± 0.10	-18.74 ± 0.03
H

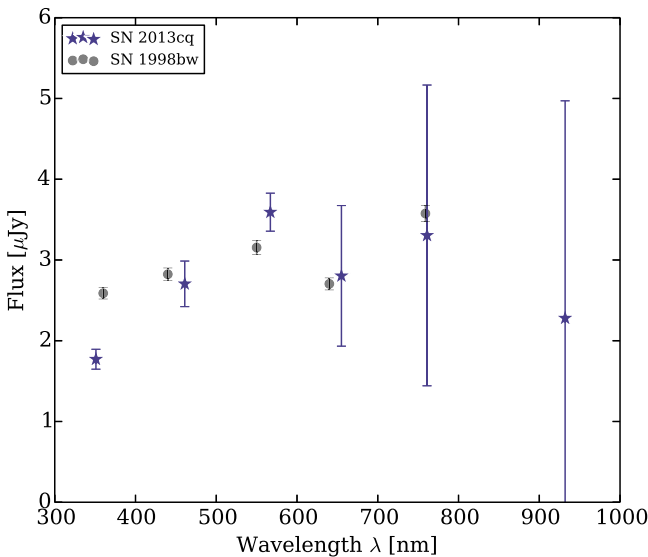


Figure 10. Broadband rest-frame SED of SN 2013cq (stars) and SN 1998bw (circles) by averaging their fluxes from days 18 to 26. The wavelength is in the rest-frame, but the flux density is observed for SN 2013cq and shifted to $z = 0.34$ for SN 1998bw.

errors were calculated using the standard deviation of the best-fit parameters after Gaussian perturbations around the flux values observed over 10,000 trials. Table 7 shows the residuals to the fit in the sense of data minus model in units of μJy .

3.3. Late Afterglow ($t > 0.7$ days)

To characterize the late afterglow ($t > 0.7$ days), we use the $grizYHJ$ flux densities from our PSF-fitting photometry of the subtracted images from Table 6. We fitted with a model $F = A_L t^{-\alpha_L}$, in which F is the flux density in each filter, A_L is a constant, t is the time since the BAT trigger (in days) and α_L is the temporal index, assumed to be the same for all filters. The model has eight free parameters: the seven values of A_L and the one value of the index α_L .

Again, we minimized the value of χ^2 to find the best-fit parameters. To avoid the worst contamination from the SN, we fitted only the data points from 0.7 to 7 days and from 40 days onward. The final fit has a $\chi^2/n = 1.05$ with $n = 327$ degrees of freedom. The best-fit parameters are given in Table 3. The errors were calculated using the standard deviation of the best-fit parameters with Gaussian perturbations to the flux value and 10,000 trials. Figures 2–8 show the data and the best fit.

Table 8 shows the residuals to the fit in the sense of data minus model in units of μJy .

4. Results

4.1. SN Component

The host-subtracted measurements minus the the best-fit afterglow models (Table 8), henceforth residuals, are show in Figures 2–8. These residuals show a rise and fall from about 7 to about 40 days, confirming the suggestion of Watson et al. (2013). We propose that this is the photometric signature of SN 2013cq.

To compare our data to SN 1988bw at a redshift of $z = 0.0085$ (Tinney et al. 1998), we need to account for the effects of redshift on the luminosity distance, observed band, and time dilation. For the luminosity distance, we used a ΛCDM model with a $H_0 = 67.8 \text{ km Mpc}^{-1} \text{ s}^{-1}$ (Planck Collaboration et al. 2014). The effect of redshift on the filters is shown in Table 4. In this table, the first and second column give the RATIR filter and its central wavelength $\bar{\lambda}$ at $z = 0$, the third column gives the central wavelength $\bar{\lambda}$ in the rest-frame of SN 2013cq at $z = 0.34$, and the fourth and fifth give the corresponding Johnson–Cousins filters and their central wavelengths at $z = 0$. Fortuitously, there is a good correspondence between the RATIR $griZYH$ filters at $z = 0.34$ and the Johnson $UBVRIJ$ filters at $z \approx 0$. The time dilation correction is a factor of $(1 + 0.34)/(1 + 0.0085) = 1.33$.

Figure 9 compares our photometry of SN 2013cq with that of SN 1998bw shifted to $z = 0.34$ (Galama et al. 1998; Foley et al. 2006; Clocchiatti et al. 2011), both bands in the rest-frame. Qualitatively, the agreement is good, especially in the bluer $griz$ filters, although compared with SN 1998bw, SN 2013cq is fainter in the g -band while it is brighter in the riz filters.

The peak times, calculated by adjusting third-degree polynomials to the residuals (between 7 and 40 days), are 17.66, 17.33, and 22.00 days, with χ^2/dof of 0.62, 0.92, and 0.06, respectively, for the g , r , and i bands, and are consistent with Xu et al. (2013a). A similar fit to the Z band did not produce a convincing fit (the reduced χ^2/dof was 5.44), so we do not have confidence in the peak time for that band.

Moreover, Figure 9 also compares our residuals with the P60 (Perley et al. 2014), NOT (Xu et al. 2013a), and VLT (Melandri et al. 2014) photometry. This shows the superior temporal coverage of the RATIR data (we have photometry for every night from nights 5 to 40) and the lower noise. For example, the errors (associated with the observations) in our residuals, calculated around the SN peak in the r -band (between 18 and 26 days after the GRB trigger) are around $0.48 \mu\text{Jy}$, while Perley et al. (2014), Xu et al. (2013a), and Melandri et al. (2014) give estimated errors of 1.7, 1.5, and $0.7 \mu\text{Jy}$ for their photometry with P60, NOT, and VLT, respectively.

We determined the peak flux density and magnitudes of SN 2013cq and SN 1998bw shifted to $z = 0.34$, by averaging the residuals from days 18 to 26. These are given in Table 5. The SEDs at the peak flux of both supernovae are shown in Figure 10. Within our considerable uncertainties, the broadband SED of SN 2013cq is compatible with that of SN 1998bw for 300–800 nm and suggest similarities in the ejected ^{56}Ni masses and kinetic energies between both SNe. For SN 2013cq the rest-frame M_r magnitude (from our observed Z magnitude)

Table 6
Photometry of GRB 130427A

t_0 (day)	t_0 (s)	t_e (s)	t_f (s)	Filter	m (AB) (Aperture)	Flux (μ Jy) (PSF)
0.01	930	80	0.01	<i>i</i>	12.88 ± 0.02	...
0.01	1009	67	0.01	Z	12.75 ± 0.02	...
0.01	1012	67	0.01	J	12.69 ± 0.02	...
0.01	1037	80	0.01	<i>i</i>	12.97 ± 0.02	...
0.01	1111	67	0.01	H	12.86 ± 0.02	...
0.01	1114	67	0.01	Y	12.77 ± 0.02	...
0.01	1141	80	0.01	<i>i</i>	13.12 ± 0.02	...
0.01	1216	67	0.01	Y	12.88 ± 0.02	...
0.01	1216	67	0.01	H	13.00 ± 0.02	...
0.01	1249	80	0.02	<i>i</i>	13.24 ± 0.02	...
0.02	1323	67	0.02	Z	13.10 ± 0.02	...
0.02	1326	67	0.02	J	13.01 ± 0.02	...
0.02	1348	80	0.02	<i>i</i>	13.35 ± 0.02	...
0.02	1429	67	0.02	J	13.14 ± 0.02	...
0.02	1432	67	0.02	Z	13.22 ± 0.02	...
0.02	1458	80	0.02	<i>i</i>	13.42 ± 0.02	...
0.02	1532	67	0.02	H	13.21 ± 0.03	...
0.02	1534	67	0.02	Y	13.20 ± 0.02	...
0.02	1579	80	0.02	<i>i</i>	13.51 ± 0.02	...
0.02	1653	67	0.02	H	13.26 ± 0.02	...
0.02	1653	67	0.02	Y	13.28 ± 0.02	...
0.02	1684	80	0.02	<i>i</i>	13.55 ± 0.02	...
0.02	1762	67	0.02	Z	13.43 ± 0.02	...
0.02	1764	67	0.02	J	13.37 ± 0.02	...
0.02	1778	80	0.02	<i>i</i>	13.61 ± 0.02	...
0.02	1858	67	0.02	J	13.40 ± 0.02	...
0.02	1859	67	0.02	Z	13.50 ± 0.02	...
0.02	1888	80	0.02	<i>i</i>	13.70 ± 0.02	...
0.02	1962	67	0.02	Y	13.47 ± 0.02	...
0.02	1964	67	0.02	H	13.43 ± 0.03	...
0.02	1993	80	0.02	<i>i</i>	13.72 ± 0.02	...
0.02	2067	67	0.02	Y	13.53 ± 0.02	...
0.02	2068	67	0.02	H	13.48 ± 0.03	...
0.02	2121	80	0.03	<i>i</i>	13.87 ± 0.02	...
0.03	2196	67	0.03	J	13.59 ± 0.02	...
0.03	2196	67	0.03	Z	13.69 ± 0.02	...
0.03	2224	80	0.03	<i>i</i>	13.87 ± 0.02	...
0.03	2298	67	0.03	J	13.64 ± 0.02	...
0.03	2300	67	0.03	Z	13.73 ± 0.02	...
0.03	2329	80	0.03	<i>i</i>	13.89 ± 0.02	...
0.03	2408	67	0.03	H	13.67 ± 0.02	...
0.03	2408	67	0.03	Y	13.70 ± 0.02	...
0.03	2422	80	0.03	<i>i</i>	13.98 ± 0.02	...
0.03	2502	67	0.03	Y	13.76 ± 0.02	...
0.03	2506	67	0.03	H	13.72 ± 0.02	...
0.03	2531	80	0.03	<i>i</i>	14.03 ± 0.02	...
0.03	2605	67	0.03	J	13.81 ± 0.02	...
0.03	2607	67	0.03	Z	13.88 ± 0.02	...
0.03	2655	80	0.03	<i>i</i>	14.07 ± 0.02	...
0.03	2729	67	0.03	J	13.88 ± 0.02	...
0.03	2732	67	0.03	Z	13.97 ± 0.02	...
0.03	2780	80	0.03	<i>i</i>	14.15 ± 0.02	...
0.03	2855	67	0.03	Y	13.89 ± 0.02	...
0.03	2856	67	0.03	H	13.87 ± 0.03	...
0.03	2885	80	0.03	<i>i</i>	14.14 ± 0.02	...
0.03	2960	67	0.04	Y	13.93 ± 0.02	...
0.03	2961	67	0.04	H	13.85 ± 0.03	...
0.03	2990	80	0.04	<i>i</i>	14.19 ± 0.02	...
0.04	3067	67	0.04	Z	14.06 ± 0.02	...
0.04	3069	67	0.04	J	14.00 ± 0.02	...
0.04	3108	80	0.04	<i>i</i>	14.25 ± 0.02	...
0.04	3186	67	0.04	J	14.06 ± 0.02	...
0.04	3186	67	0.04	Z	14.15 ± 0.02	...

Table 6
(Continued)

t_0 (day)	t_0 (s)	t_e (s)	t_f (s)	Filter	m (AB) (Aperture)	Flux (μJy) (PSF)
0.04	3214	80	0.04	<i>i</i>	14.28 ± 0.02	...
0.04	3292	67	0.04	<i>Y</i>	14.06 ± 0.02	...
0.04	3293	67	0.04	<i>H</i>	13.99 ± 0.03	...
0.04	3307	80	0.04	<i>i</i>	14.31 ± 0.02	...
0.04	3387	67	0.04	<i>H</i>	14.03 ± 0.03	...
0.04	3389	67	0.04	<i>Y</i>	14.08 ± 0.02	...
0.04	3418	80	0.04	<i>i</i>	14.32 ± 0.02	...
0.04	3493	67	0.04	<i>J</i>	14.19 ± 0.02	...
0.04	3493	67	0.04	<i>Z</i>	14.24 ± 0.02	...
0.04	3535	80	0.04	<i>i</i>	14.35 ± 0.02	...
0.04	3610	67	0.04	<i>Z</i>	14.22 ± 0.02	...
0.04	3611	67	0.04	<i>J</i>	14.17 ± 0.02	...
0.04	3640	80	0.04	<i>i</i>	14.40 ± 0.02	...
0.04	3719	67	0.04	<i>H</i>	14.09 ± 0.03	...
0.04	3721	67	0.04	<i>Y</i>	14.16 ± 0.02	...
0.04	3736	80	0.04	<i>i</i>	14.41 ± 0.02	...
0.04	3814	67	0.04	<i>Y</i>	14.21 ± 0.02	...
0.04	3815	67	0.04	<i>H</i>	14.12 ± 0.03	...
0.04	3843	80	0.05	<i>i</i>	14.44 ± 0.02	...
0.05	3918	67	0.05	<i>J</i>	14.28 ± 0.03	...
0.05	3919	67	0.05	<i>Z</i>	14.33 ± 0.02	...
0.05	3964	80	0.05	<i>i</i>	14.45 ± 0.02	...
0.05	4038	67	0.05	<i>J</i>	14.25 ± 0.02	...
0.05	4038	67	0.05	<i>Z</i>	14.32 ± 0.02	...
0.05	4145	67	0.05	<i>H</i>	14.23 ± 0.03	...
0.05	4146	67	0.05	<i>Y</i>	14.26 ± 0.02	...
0.05	4172	80	0.05	<i>i</i>	14.51 ± 0.02	...
0.05	4247	67	0.05	<i>H</i>	14.24 ± 0.03	...
0.05	4248	67	0.05	<i>Y</i>	14.28 ± 0.02	...
0.05	4295	80	0.05	<i>i</i>	14.55 ± 0.02	...
0.05	4371	67	0.05	<i>J</i>	14.33 ± 0.02	...
0.05	4371	67	0.05	<i>Z</i>	14.40 ± 0.02	...
0.05	4415	80	0.05	<i>i</i>	14.56 ± 0.02	...
0.05	4493	67	0.05	<i>J</i>	14.36 ± 0.02	...
0.05	4493	67	0.05	<i>Z</i>	14.44 ± 0.02	...
0.05	4523	80	0.05	<i>i</i>	14.76 ± 0.03	...
0.05	4598	67	0.05	<i>H</i>	14.39 ± 0.07	...
0.05	4598	67	0.05	<i>Y</i>	14.45 ± 0.03	...
0.05	4643	80	0.05	<i>i</i>	14.59 ± 0.02	...
0.05	4718	67	0.06	<i>Y</i>	14.40 ± 0.02	...
0.05	4719	67	0.06	<i>H</i>	14.38 ± 0.03	...
0.05	4742	80	0.06	<i>i</i>	14.64 ± 0.02	...
0.06	4821	67	0.06	<i>J</i>	14.46 ± 0.02	...
0.06	4822	67	0.06	<i>Z</i>	14.51 ± 0.02	...
0.06	4847	80	0.06	<i>i</i>	14.66 ± 0.02	...
0.06	4922	67	0.06	<i>J</i>	14.48 ± 0.02	...
0.06	4923	67	0.06	<i>Z</i>	14.89 ± 0.02	...
0.06	4954	80	0.06	<i>i</i>	14.68 ± 0.02	...
0.06	5028	67	0.06	<i>H</i>	14.33 ± 0.05	...
0.06	5032	67	0.06	<i>Y</i>	14.44 ± 0.03	...
0.06	5059	80	0.06	<i>i</i>	14.70 ± 0.02	...
0.06	5134	67	0.06	<i>H</i>	14.42 ± 0.03	...
0.06	5135	67	0.06	<i>Y</i>	14.45 ± 0.02	...
0.06	5186	80	0.06	<i>i</i>	14.75 ± 0.03	...
0.06	5260	67	0.06	<i>J</i>	14.53 ± 0.02	...
0.06	5262	67	0.06	<i>Z</i>	14.57 ± 0.02	...
0.06	5288	80	0.06	<i>i</i>	14.71 ± 0.02	...
0.06	5362	67	0.06	<i>J</i>	14.54 ± 0.02	...
0.06	5362	67	0.06	<i>Z</i>	14.59 ± 0.02	...
0.06	5395	80	0.06	<i>i</i>	14.76 ± 0.02	...
0.06	5470	67	0.06	<i>H</i>	14.43 ± 0.04	...
0.06	5470	67	0.06	<i>Y</i>	14.52 ± 0.02	...
0.06	5506	80	0.06	<i>i</i>	14.79 ± 0.02	...

Table 6
(Continued)

t_0 (day)	t_0 (s)	t_e (s)	t_f (s)	Filter	m (AB) (Aperture)	Flux (μ Jy) (PSF)
0.06	5586	67	0.07	<i>H</i>	14.47 ± 0.03	...
0.06	5586	67	0.07	<i>Y</i>	14.56 ± 0.02	...
0.06	5615	80	0.07	<i>i</i>	14.78 ± 0.02	...
0.07	5690	67	0.07	<i>J</i>	14.58 ± 0.02	...
0.07	5694	67	0.07	<i>Z</i>	14.69 ± 0.02	...
0.07	5715	80	0.07	<i>i</i>	14.79 ± 0.02	...
0.07	5789	67	0.07	<i>J</i>	14.58 ± 0.02	...
0.07	5790	67	0.07	<i>Z</i>	14.65 ± 0.02	...
0.07	5823	80	0.07	<i>i</i>	14.80 ± 0.02	...
0.07	5897	67	0.07	<i>H</i>	14.53 ± 0.02	...
0.07	5898	67	0.07	<i>Y</i>	14.62 ± 0.02	...
0.07	5943	80	0.07	<i>i</i>	14.89 ± 0.03	...
0.07	6018	67	0.07	<i>Y</i>	14.61 ± 0.02	...
0.07	6020	67	0.07	<i>H</i>	14.51 ± 0.03	...
0.07	6051	80	0.07	<i>i</i>	14.86 ± 0.02	...
0.07	6124	67	0.07	<i>J</i>	14.66 ± 0.02	...
0.07	6125	67	0.07	<i>Z</i>	14.73 ± 0.02	...
0.83	71485	1280	0.85	<i>i</i>	17.45 ± 0.42	374.99 ± 12.58
0.83	71485	1280	0.85	<i>r</i>	17.59 ± 0.42	327.32 ± 13.34
0.83	71489	536	0.85	<i>Y</i>	17.12 ± 0.42	519.07 ± 89.32
0.83	71489	536	0.85	<i>Z</i>	17.23 ± 0.42	459.20 ± 82.36
0.83	71490	536	0.85	<i>H</i>	17.01 ± 0.42	584.25 ± 104.51
0.83	71490	536	0.85	<i>J</i>	17.14 ± 0.42	489.86 ± 118.33
0.85	73170	1280	0.87	<i>i</i>	17.48 ± 0.42	360.45 ± 12.42
0.85	73170	1280	0.87	<i>r</i>	17.61 ± 0.42	319.00 ± 16.78
0.85	73171	536	0.87	<i>Y</i>	17.11 ± 0.42	519.29 ± 106.76
0.85	73171	536	0.87	<i>Z</i>	17.26 ± 0.42	444.71 ± 97.80
0.85	73173	536	0.87	<i>H</i>	17.04 ± 0.42	572.18 ± 298.77
0.85	73173	536	0.87	<i>J</i>	17.16 ± 0.42	482.33 ± 99.53
0.87	74870	1280	0.89	<i>i</i>	17.50 ± 0.42	361.40 ± 11.22
0.87	74870	1280	0.89	<i>r</i>	17.66 ± 0.42	307.57 ± 6.73
0.87	74872	536	0.89	<i>H</i>	17.02 ± 0.42	556.82 ± 94.64
0.87	74872	536	0.89	<i>J</i>	17.19 ± 0.42	492.18 ± 98.82
0.87	74873	536	0.89	<i>Y</i>	17.14 ± 0.42	492.73 ± 91.88
0.87	74873	536	0.89	<i>Z</i>	17.29 ± 0.42	434.49 ± 62.79
0.90	77485	1280	0.92	<i>r</i>	17.71 ± 0.42	297.70 ± 17.58
0.90	77485	1280	0.92	<i>i</i>	17.56 ± 0.42	335.92 ± 15.12
0.90	77490	536	0.92	<i>Y</i>	17.27 ± 0.42	451.80 ± 55.35
0.90	77490	536	0.92	<i>Z</i>	17.32 ± 0.42	413.81 ± 67.52
0.90	77491	536	0.92	<i>H</i>	17.14 ± 0.42	520.21 ± 61.26
0.90	77491	536	0.92	<i>J</i>	17.25 ± 0.42	456.95 ± 65.92
0.92	79150	1280	0.93	<i>i</i>	17.59 ± 0.42	329.32 ± 11.05
0.92	79150	1280	0.93	<i>r</i>	17.76 ± 0.42	281.54 ± 8.12
0.92	79151	536	0.93	<i>Y</i>	17.28 ± 0.42	466.42 ± 62.22
0.92	79151	536	0.93	<i>Z</i>	17.36 ± 0.42	399.12 ± 62.30
0.92	79151	536	0.93	<i>H</i>	17.11 ± 0.42	539.28 ± 76.97
0.92	79151	536	0.93	<i>J</i>	17.33 ± 0.42	412.45 ± 54.73
0.94	80826	1280	0.95	<i>i</i>	17.62 ± 0.42	314.80 ± 10.13
0.94	80826	1280	0.95	<i>r</i>	17.77 ± 0.42	275.47 ± 8.21
0.94	80827	536	0.95	<i>Y</i>	17.26 ± 0.42	441.59 ± 64.98
0.94	80827	536	0.95	<i>Z</i>	17.41 ± 0.42	391.78 ± 29.23
0.94	80828	536	0.95	<i>H</i>	17.17 ± 0.42	551.47 ± 69.19
0.94	80828	536	0.95	<i>J</i>	17.26 ± 0.42	437.22 ± 73.40
0.97	83586	1280	0.99	<i>i</i>	17.65 ± 0.42	306.26 ± 11.71
0.97	83586	1280	0.99	<i>r</i>	17.81 ± 0.42	267.65 ± 10.62
0.97	83593	536	0.99	<i>H</i>	17.23 ± 0.42	504.95 ± 57.64
0.97	83593	536	0.99	<i>J</i>	17.35 ± 0.42	411.12 ± 57.56
0.97	83632	536	0.99	<i>Y</i>	17.30 ± 0.42	427.96 ± 57.65
0.97	83632	536	0.99	<i>Z</i>	17.42 ± 0.42	380.83 ± 41.56
0.99	85331	1280	1.01	<i>i</i>	17.69 ± 0.42	295.68 ± 8.70
0.99	85331	1280	1.01	<i>r</i>	17.84 ± 0.42	260.68 ± 13.34
0.99	85333	536	1.01	<i>Y</i>	17.37 ± 0.42	401.57 ± 43.58
0.99	85333	536	1.01	<i>Z</i>	17.43 ± 0.42	372.94 ± 56.57

Table 6
(Continued)

t_0 (day)	t_0 (s)	t_e (s)	t_f (s)	Filter	m (AB) (Aperture)	Flux (μ Jy) (PSF)
0.99	85333	536	1.01	<i>H</i>	17.23 ± 0.42	507.92 ± 63.59
0.99	85333	536	1.01	<i>J</i>	17.38 ± 0.42	395.39 ± 53.28
1.01	87061	1280	1.03	<i>r</i>	17.84 ± 0.42	258.40 ± 11.61
1.01	87061	1280	1.03	<i>i</i>	17.73 ± 0.42	285.60 ± 10.05
1.01	87064	536	1.03	<i>Y</i>	17.40 ± 0.42	401.01 ± 52.93
1.01	87064	536	1.03	<i>Z</i>	17.49 ± 0.42	362.49 ± 54.65
1.01	87066	536	1.03	<i>H</i>	17.25 ± 0.42	466.24 ± 60.97
1.01	87066	536	1.03	<i>J</i>	17.38 ± 0.42	400.08 ± 54.92
1.04	89861	1280	1.06	<i>i</i>	17.76 ± 0.42	278.74 ± 9.38
1.04	89861	1280	1.06	<i>r</i>	17.90 ± 0.42	243.80 ± 9.30
1.04	89867	536	1.06	<i>Y</i>	17.41 ± 0.42	382.43 ± 51.77
1.04	89867	536	1.06	<i>Z</i>	17.50 ± 0.42	348.99 ± 96.74
1.04	89871	536	1.06	<i>H</i>	17.33 ± 0.42	437.23 ± 106.18
1.04	89871	536	1.06	<i>J</i>	17.41 ± 0.42	380.89 ± 75.30
1.06	91596	1280	1.08	<i>i</i>	17.78 ± 0.42	271.33 ± 9.76
1.06	91596	1280	1.08	<i>r</i>	17.94 ± 0.42	231.70 ± 13.04
1.06	91600	536	1.08	<i>H</i>	17.28 ± 0.42	445.08 ± 108.89
1.06	91600	536	1.08	<i>J</i>	17.45 ± 0.42	375.58 ± 86.51
1.06	91600	536	1.08	<i>Y</i>	17.41 ± 0.42	376.09 ± 57.58
1.06	91600	536	1.08	<i>Z</i>	17.58 ± 0.42	317.29 ± 72.73
1.83	157967	1280	1.85	<i>r</i>	18.70 ± 0.42	113.69 ± 1.72
1.83	157967	1280	1.85	<i>i</i>	18.53 ± 0.42	132.35 ± 3.46
1.83	157972	536	1.85	<i>H</i>	18.05 ± 0.43	219.71 ± 76.44
1.83	157972	536	1.85	<i>J</i>	18.23 ± 0.43	173.86 ± 53.15
1.83	157972	536	1.85	<i>Y</i>	18.08 ± 0.42	192.81 ± 23.85
1.83	157972	536	1.85	<i>Z</i>	18.25 ± 0.42	169.00 ± 20.03
1.85	159663	1280	1.87	<i>r</i>	18.70 ± 0.42	110.99 ± 1.53
1.85	159663	1280	1.87	<i>i</i>	18.55 ± 0.42	130.24 ± 3.16
1.85	159666	536	1.87	<i>H</i>	18.06 ± 0.43	206.18 ± 67.93
1.85	159666	536	1.87	<i>J</i>	18.21 ± 0.43	175.43 ± 44.56
1.85	159668	536	1.87	<i>Y</i>	18.12 ± 0.42	188.45 ± 27.83
1.85	159668	536	1.87	<i>Z</i>	18.34 ± 0.42	158.21 ± 15.76
1.87	161334	1280	1.89	<i>i</i>	18.55 ± 0.42	129.04 ± 2.97
1.87	161334	1280	1.89	<i>r</i>	18.72 ± 0.42	110.25 ± 1.77
1.87	161335	536	1.89	<i>Y</i>	18.11 ± 0.42	185.62 ± 27.80
1.87	161335	536	1.89	<i>Z</i>	18.34 ± 0.42	153.69 ± 17.65
1.87	161337	536	1.89	<i>H</i>	18.08 ± 0.43	215.43 ± 78.45
1.87	161337	536	1.89	<i>J</i>	18.23 ± 0.43	169.34 ± 41.59
1.89	163694	1280	1.91	<i>i</i>	18.57 ± 0.42	125.75 ± 1.90
1.89	163694	1280	1.91	<i>r</i>	18.72 ± 0.42	109.57 ± 1.17
1.89	163700	536	1.91	<i>Y</i>	18.19 ± 0.42	178.61 ± 17.89
1.89	163700	536	1.91	<i>Z</i>	18.35 ± 0.42	157.04 ± 13.47
1.89	163702	536	1.91	<i>H</i>	18.06 ± 0.43	219.76 ± 61.30
1.89	163702	536	1.91	<i>J</i>	18.34 ± 0.42	163.73 ± 28.56
1.91	165405	1280	1.93	<i>i</i>	18.60 ± 0.42	124.18 ± 2.92
1.91	165405	1280	1.93	<i>r</i>	18.77 ± 0.42	105.43 ± 1.43
1.91	165407	536	1.93	<i>Y</i>	18.20 ± 0.42	177.57 ± 18.95
1.91	165407	536	1.93	<i>Z</i>	18.36 ± 0.42	153.59 ± 12.91
1.91	165408	536	1.93	<i>H</i>	18.14 ± 0.43	198.83 ± 46.64
1.91	165408	536	1.93	<i>J</i>	18.30 ± 0.42	166.47 ± 29.66
1.93	167079	1280	1.95	<i>i</i>	18.60 ± 0.42	122.24 ± 2.87
1.93	167079	1280	1.95	<i>r</i>	18.76 ± 0.42	104.86 ± 2.11
1.93	167081	536	1.95	<i>H</i>	18.06 ± 0.42	209.93 ± 56.56
1.93	167081	536	1.95	<i>J</i>	18.28 ± 0.42	164.50 ± 26.93
1.93	167081	536	1.95	<i>Y</i>	18.23 ± 0.42	172.74 ± 18.35
1.93	167081	536	1.95	<i>Z</i>	18.39 ± 0.42	152.73 ± 12.78
1.96	169250	536	1.98	<i>H</i>	18.04 ± 0.42	209.45 ± 45.11
1.96	169250	536	1.98	<i>J</i>	18.34 ± 0.42	161.81 ± 61.05
1.96	169286	1280	1.98	<i>r</i>	18.78 ± 0.42	104.67 ± 2.68
1.96	169286	1280	1.98	<i>i</i>	18.62 ± 0.42	120.64 ± 2.56
1.96	169310	469	1.98	<i>Y</i>	18.29 ± 0.42	173.81 ± 21.84
1.96	169310	604	1.98	<i>Z</i>	18.36 ± 0.42	153.08 ± 13.55
1.98	170985	1280	2.00	<i>i</i>	18.63 ± 0.42	120.42 ± 2.36

Table 6
(Continued)

t_0 (day)	t_0 (s)	t_e (s)	t_f (s)	Filter	m (AB) (Aperture)	Flux (μJy) (PSF)
1.98	170985	1280	2.00	<i>r</i>	18.80 \pm 0.42	101.31 \pm 2.98
1.98	170986	536	2.00	<i>H</i>	18.04 \pm 0.43	230.80 \pm 110.74
1.98	170986	536	2.00	<i>J</i>	18.23 \pm 0.42	164.63 \pm 30.78
1.98	171108	536	2.00	<i>Y</i>	18.21 \pm 0.42	180.27 \pm 22.90
1.98	171108	536	2.00	<i>Z</i>	18.45 \pm 0.42	142.52 \pm 16.11
2.00	172728	1280	2.02	<i>r</i>	18.82 \pm 0.42	98.70 \pm 1.90
2.00	172728	1280	2.02	<i>i</i>	18.62 \pm 0.42	120.02 \pm 2.87
2.00	172735	536	2.02	<i>H</i>	18.10 \pm 0.43	219.87 \pm 63.24
2.00	172735	536	2.02	<i>J</i>	18.37 \pm 0.43	154.87 \pm 31.02
2.00	173091	536	2.03	<i>Y</i>	18.28 \pm 0.42	159.93 \pm 21.83
2.00	173091	536	2.03	<i>Z</i>	18.37 \pm 0.42	152.26 \pm 18.02
2.02	174940	1280	2.04	<i>r</i>	18.83 \pm 0.42	97.36 \pm 2.12
2.02	174940	1280	2.04	<i>i</i>	18.65 \pm 0.42	117.40 \pm 2.51
2.02	174946	536	2.04	<i>H</i>	18.23 \pm 0.43	191.66 \pm 95.17
2.02	174946	536	2.04	<i>J</i>	18.31 \pm 0.43	163.10 \pm 44.53
2.03	175056	536	2.05	<i>Y</i>	18.32 \pm 0.42	157.62 \pm 25.69
2.03	175056	536	2.05	<i>Z</i>	18.41 \pm 0.42	146.81 \pm 18.00
2.04	176669	1280	2.06	<i>i</i>	18.68 \pm 0.42	114.04 \pm 4.09
2.04	176669	1280	2.06	<i>r</i>	18.85 \pm 0.42	97.26 \pm 2.93
2.04	176673	536	2.06	<i>H</i>	18.14 \pm 0.43	209.82 \pm 125.97
2.04	176673	536	2.06	<i>J</i>	18.35 \pm 0.43	161.18 \pm 52.20
2.83	244162	1280	2.85	<i>i</i>	19.15 \pm 0.42	71.80 \pm 1.38
2.83	244162	1280	2.85	<i>r</i>	19.28 \pm 0.42	62.18 \pm 0.91
2.83	244168	536	2.85	<i>H</i>	18.49 \pm 0.43	135.44 \pm 80.88
2.83	244168	536	2.85	<i>J</i>	18.81 \pm 0.43	94.62 \pm 40.25
2.83	244171	536	2.85	<i>Y</i>	18.72 \pm 0.43	114.77 \pm 24.01
2.83	244171	536	2.85	<i>Z</i>	18.84 \pm 0.42	95.64 \pm 8.66
2.85	245865	1280	2.86	<i>i</i>	19.13 \pm 0.42	72.81 \pm 1.67
2.85	245865	1280	2.86	<i>r</i>	19.26 \pm 0.42	63.45 \pm 1.38
2.85	245867	469	2.86	<i>H</i>	18.51 \pm 0.43	117.37 \pm 133.41
2.85	245867	536	2.86	<i>Y</i>	18.67 \pm 0.43	109.85 \pm 23.93
2.85	245867	536	2.86	<i>Z</i>	18.92 \pm 0.42	88.60 \pm 9.96
2.85	245867	604	2.86	<i>J</i>	18.81 \pm 0.43	100.35 \pm 55.57
2.87	247553	1280	2.88	<i>i</i>	19.14 \pm 0.42	71.86 \pm 1.42
2.87	247553	1280	2.88	<i>r</i>	19.28 \pm 0.42	63.17 \pm 0.93
2.87	247555	536	2.88	<i>Y</i>	18.66 \pm 0.43	116.44 \pm 25.16
2.87	247555	536	2.88	<i>Z</i>	18.91 \pm 0.42	91.74 \pm 8.23
2.87	247556	536	2.88	<i>H</i>	18.56 \pm 0.43	130.53 \pm 76.23
2.87	247556	536	2.88	<i>J</i>	18.86 \pm 0.43	95.17 \pm 31.71
2.89	249656	536	2.91	<i>H</i>	18.72 \pm 0.43	116.01 \pm 48.13
2.89	249656	536	2.91	<i>J</i>	18.89 \pm 0.43	88.72 \pm 22.27
2.89	249656	536	2.91	<i>Y</i>	18.81 \pm 0.43	94.88 \pm 11.61
2.89	249656	536	2.91	<i>Z</i>	18.86 \pm 0.42	92.86 \pm 5.93
2.89	249693	1280	2.91	<i>i</i>	19.16 \pm 0.42	70.79 \pm 1.21
2.89	249693	1280	2.91	<i>r</i>	19.31 \pm 0.42	61.72 \pm 1.09
2.91	251349	1280	2.93	<i>i</i>	19.16 \pm 0.42	69.79 \pm 1.31
2.91	251349	1280	2.93	<i>r</i>	19.32 \pm 0.42	60.07 \pm 1.05
2.91	251350	536	2.93	<i>Y</i>	18.76 \pm 0.43	99.00 \pm 15.22
2.91	251350	536	2.93	<i>Z</i>	18.94 \pm 0.42	84.23 \pm 7.06
2.91	251352	536	2.93	<i>H</i>	18.70 \pm 0.43	118.01 \pm 54.31
2.91	251352	536	2.93	<i>J</i>	18.88 \pm 0.43	93.52 \pm 23.21
2.93	253022	1280	2.95	<i>i</i>	19.18 \pm 0.42	69.02 \pm 1.33
2.93	253022	1280	2.95	<i>r</i>	19.33 \pm 0.42	59.30 \pm 1.37
2.93	253024	536	2.95	<i>Y</i>	18.77 \pm 0.43	97.99 \pm 25.24
2.93	253024	536	2.95	<i>Z</i>	18.94 \pm 0.42	85.20 \pm 7.17
2.93	253024	536	2.95	<i>H</i>	18.60 \pm 0.43	130.78 \pm 58.04
2.93	253024	536	2.95	<i>J</i>	18.86 \pm 0.43	96.18 \pm 22.58
2.95	255197	536	2.97	<i>Y</i>	18.70 \pm 0.43	104.72 \pm 17.90
2.95	255197	536	2.97	<i>Z</i>	18.89 \pm 0.42	88.48 \pm 7.17
2.95	255199	536	2.97	<i>H</i>	18.70 \pm 0.43	120.87 \pm 62.41
2.95	255199	536	2.97	<i>J</i>	18.85 \pm 0.43	98.59 \pm 21.59
2.95	255236	1280	2.97	<i>r</i>	19.36 \pm 0.42	58.44 \pm 1.39
2.95	255236	1280	2.97	<i>i</i>	19.18 \pm 0.42	68.25 \pm 1.39

Table 6
(Continued)

t_0 (day)	t_0 (s)	t_e (s)	t_f (s)	Filter	m (AB) (Aperture)	Flux (μJy) (PSF)
2.97	256928	1280	2.99	<i>r</i>	19.38 ± 0.42	57.44 ± 1.10
2.97	256930	1280	2.99	<i>i</i>	19.19 ± 0.42	67.23 ± 1.40
2.97	256934	536	2.99	<i>H</i>	18.66 ± 0.43	137.34 ± 72.34
2.97	256934	536	2.99	<i>J</i>	18.92 ± 0.43	91.18 ± 22.10
2.97	256936	536	2.99	<i>Y</i>	18.77 ± 0.43	98.98 ± 17.71
2.97	256936	536	2.99	<i>Z</i>	19.03 ± 0.42	82.69 ± 8.79
2.99	258662	1280	3.01	<i>i</i>	19.17 ± 0.42	69.61 ± 1.43
2.99	258662	1280	3.01	<i>r</i>	19.37 ± 0.42	57.93 ± 1.33
2.99	258663	536	3.01	<i>Y</i>	18.74 ± 0.43	102.65 ± 22.76
2.99	258663	536	3.01	<i>Z</i>	18.96 ± 0.42	80.52 ± 9.23
2.99	258664	536	3.01	<i>H</i>	18.68 ± 0.43	112.91 ± 91.56
2.99	258664	536	3.01	<i>J</i>	18.80 ± 0.43	93.21 ± 27.34
3.02	260909	536	3.04	<i>Y</i>	18.72 ± 0.43	101.24 ± 20.76
3.02	260909	536	3.04	<i>Z</i>	18.93 ± 0.42	81.85 ± 8.58
3.02	260910	536	3.04	<i>H</i>	18.67 ± 0.43	123.48 ± 84.77
3.02	260910	536	3.04	<i>J</i>	18.83 ± 0.43	96.51 ± 26.43
3.02	260945	1280	3.04	<i>r</i>	19.40 ± 0.42	54.45 ± 1.09
3.02	260945	1280	3.04	<i>i</i>	19.19 ± 0.42	69.98 ± 1.71
3.04	262654	1280	3.06	<i>i</i>	19.23 ± 0.42	65.45 ± 1.41
3.04	262654	1280	3.06	<i>r</i>	19.36 ± 0.42	58.12 ± 1.37
3.04	262658	536	3.06	<i>H</i>	18.57 ± 0.43	123.33 ± 90.72
3.04	262658	536	3.06	<i>J</i>	18.93 ± 0.43	89.83 ± 30.08
3.04	262659	536	3.06	<i>Y</i>	18.84 ± 0.43	94.95 ± 20.75
3.04	262659	536	3.06	<i>Z</i>	19.01 ± 0.43	81.33 ± 9.88
3.82	330101	1280	3.84	<i>r</i>	19.70 ± 0.42	40.20 ± 1.12
3.82	330102	1280	3.84	<i>i</i>	19.53 ± 0.42	47.78 ± 1.20
3.84	331631	1280	3.86	<i>r</i>	19.65 ± 0.42	41.40 ± 0.96
3.84	331631	1280	3.86	<i>i</i>	19.50 ± 0.42	48.77 ± 1.08
3.86	333148	1280	3.87	<i>r</i>	19.63 ± 0.42	41.75 ± 0.89
3.86	333148	1280	3.87	<i>i</i>	19.54 ± 0.42	47.57 ± 0.92
3.88	335229	1280	3.90	<i>r</i>	19.69 ± 0.42	40.12 ± 0.84
3.88	335229	1280	3.90	<i>i</i>	19.54 ± 0.42	47.09 ± 1.01
3.90	336754	1280	3.92	<i>r</i>	19.69 ± 0.42	39.64 ± 1.01
3.90	336754	1280	3.92	<i>i</i>	19.54 ± 0.42	45.71 ± 0.98
3.92	338278	1280	3.93	<i>r</i>	19.72 ± 0.42	40.58 ± 0.89
3.92	338279	1280	3.93	<i>i</i>	19.54 ± 0.42	46.84 ± 1.07
3.94	340206	1280	3.95	<i>r</i>	19.70 ± 0.42	39.45 ± 1.02
3.94	340206	1280	3.95	<i>i</i>	19.54 ± 0.42	46.35 ± 1.00
3.96	341738	1280	3.97	<i>r</i>	19.74 ± 0.42	38.82 ± 0.82
3.96	341738	1280	3.97	<i>i</i>	19.56 ± 0.42	46.04 ± 0.90
3.97	343270	1280	3.99	<i>r</i>	19.70 ± 0.42	39.81 ± 0.91
3.97	343271	1280	3.99	<i>i</i>	19.53 ± 0.42	47.72 ± 1.11
4.00	345316	1280	4.01	<i>r</i>	19.73 ± 0.42	38.54 ± 0.86
4.00	345316	1280	4.01	<i>i</i>	19.57 ± 0.42	45.09 ± 0.87
4.01	346882	1280	4.03	<i>r</i>	19.72 ± 0.42	39.89 ± 0.94
4.01	346882	1280	4.03	<i>i</i>	19.56 ± 0.42	47.26 ± 1.00
4.03	348470	1280	4.05	<i>r</i>	19.75 ± 0.42	38.51 ± 1.01
4.03	348471	1280	4.05	<i>i</i>	19.62 ± 0.42	44.24 ± 1.18
5.03	434444	1280	5.05	<i>g</i>	20.35 ± 0.42	21.96 ± 1.09
5.03	434467	2320	5.08	<i>r</i>	20.06 ± 0.42	25.27 ± 1.34
5.03	434468	3839	5.08	<i>i</i>	19.84 ± 0.42	33.42 ± 1.14
5.94	513072	5119	6.11	<i>r</i>	20.16 ± 0.42	23.64 ± 0.55
5.95	513912	10240	6.14	<i>i</i>	20.02 ± 0.42	27.34 ± 0.56
5.95	513920	4228	6.14	<i>Y</i>	19.68 ± 0.42	36.96 ± 2.04
5.95	513920	4295	6.14	<i>Z</i>	19.82 ± 0.42	31.53 ± 1.24
5.95	513921	4295	6.14	<i>H</i>	19.45 ± 0.43	42.74 ± 7.19
5.95	513921	4295	6.14	<i>J</i>	19.66 ± 0.42	41.53 ± 2.91
5.97	515483	5119	6.12	<i>g</i>	20.54 ± 0.42	17.98 ± 0.50
6.93	598530	12400	7.13	<i>i</i>	20.16 ± 0.42	22.37 ± 0.55
6.93	598765	11759	7.13	<i>g</i>	20.67 ± 0.42	15.46 ± 0.49
6.93	598772	4832	7.13	<i>Y</i>	19.87 ± 0.43	30.39 ± 2.19
6.93	598772	5033	7.13	<i>Z</i>	19.90 ± 0.42	28.59 ± 1.23
6.93	598776	4966	7.13	<i>H</i>	19.67 ± 0.43	32.84 ± 7.91

Table 6
(Continued)

t_0 (day)	t_0 (s)	t_e (s)	t_f (s)	Filter	m (AB) (Aperture)	Flux (μ Jy) (PSF)
6.93	598776	5033	7.13	<i>J</i>	19.82 ± 0.43	35.80 ± 5.87
7.94	686416	9040	8.14	<i>g</i>	20.82 ± 0.42	12.77 ± 0.51
7.94	686416	9679	8.14	<i>i</i>	20.31 ± 0.42	18.42 ± 0.56
7.95	686463	3557	8.14	<i>Z</i>	20.07 ± 0.43	22.98 ± 1.38
7.95	686463	3557	8.14	<i>J</i>	19.80 ± 0.43	33.50 ± 4.67
7.95	686463	4093	8.14	<i>Y</i>	19.87 ± 0.43	28.88 ± 2.74
7.95	686463	4698	8.14	<i>H</i>	19.80 ± 0.43	51.25 ± 11.57
9.96	860894	5999	10.08	<i>g</i>	21.04 ± 0.42	9.46 ± 0.49
9.96	860894	5999	10.08	<i>i</i>	20.46 ± 0.42	14.73 ± 0.57
9.96	860902	2483	10.08	<i>J</i>	20.22 ± 0.43	19.00 ± 5.64
9.96	860902	2550	10.08	<i>H</i>	20.19 ± 0.44	-1.10 ± 15.50
9.96	860904	2483	10.08	<i>Z</i>	20.18 ± 0.43	18.27 ± 1.70
9.96	860904	2550	10.08	<i>Y</i>	20.18 ± 0.43	20.30 ± 3.31
10.91	943033	1120	10.93	<i>r</i>	20.64 ± 0.43	11.51 ± 1.26
10.93	943968	3892	11.15	<i>Z</i>	20.35 ± 0.43	13.97 ± 1.59
10.93	943968	3959	11.15	<i>Y</i>	20.27 ± 0.43	18.42 ± 3.49
10.93	944062	9840	11.15	<i>i</i>	20.54 ± 0.42	13.32 ± 0.58
10.93	944113	2480	11.15	<i>g</i>	21.17 ± 0.43	8.07 ± 0.83
10.93	944130	4093	11.15	<i>J</i>	20.21 ± 0.44	24.43 ± 9.14
11.93	1030399	4832	12.13	<i>Y</i>	20.38 ± 0.43	15.22 ± 1.38
11.93	1030399	4832	12.13	<i>Z</i>	20.40 ± 0.42	13.84 ± 0.89
11.93	1030400	4832	12.13	<i>H</i>	20.09 ± 0.43	18.47 ± 4.85
11.93	1030400	4832	12.13	<i>J</i>	20.43 ± 0.43	12.27 ± 2.19
11.93	1030435	6399	12.13	<i>r</i>	20.68 ± 0.42	10.92 ± 0.52
11.93	1030435	5119	12.09	<i>g</i>	21.12 ± 0.42	8.26 ± 0.49
11.93	1030435	11519	12.13	<i>i</i>	20.58 ± 0.42	12.27 ± 0.49
12.91	1115381	5119	13.09	<i>r</i>	20.71 ± 0.42	10.44 ± 0.54
12.91	1115381	10240	13.09	<i>i</i>	20.60 ± 0.42	11.86 ± 0.50
12.91	1115386	4295	13.09	<i>Y</i>	20.33 ± 0.43	16.63 ± 1.77
12.91	1115386	4295	13.09	<i>Z</i>	20.39 ± 0.43	13.92 ± 1.02
12.91	1115413	5119	13.05	<i>g</i>	21.17 ± 0.42	7.90 ± 0.49
12.91	1115428	4295	13.09	<i>H</i>	20.34 ± 0.44	2.34 ± 6.49
12.91	1115428	4295	13.09	<i>J</i>	20.34 ± 0.43	16.98 ± 3.20
13.91	1201686	5119	14.04	<i>g</i>	21.24 ± 0.42	7.36 ± 0.48
13.91	1201710	5119	14.08	<i>r</i>	20.76 ± 0.42	9.59 ± 0.54
13.91	1201710	10160	14.08	<i>i</i>	20.67 ± 0.42	10.39 ± 0.50
13.91	1201715	4228	14.08	<i>Y</i>	20.40 ± 0.43	14.09 ± 1.74
13.91	1201715	4295	14.08	<i>Z</i>	20.52 ± 0.43	11.19 ± 0.97
13.91	1201716	4295	14.08	<i>H</i>	20.33 ± 0.44	0.08 ± 6.63
13.91	1201716	4295	14.08	<i>J</i>	20.36 ± 0.43	18.58 ± 2.92
14.90	1287710	5119	15.05	<i>r</i>	20.78 ± 0.42	9.55 ± 0.53
14.91	1288530	10240	15.08	<i>i</i>	20.72 ± 0.42	10.15 ± 0.49
14.91	1288579	4295	15.08	<i>H</i>	20.26 ± 0.43	16.57 ± 4.77
14.91	1288579	4295	15.08	<i>J</i>	20.53 ± 0.43	15.81 ± 2.29
14.91	1288581	4295	15.08	<i>Y</i>	20.41 ± 0.43	13.66 ± 1.38
14.91	1288581	4295	15.08	<i>Z</i>	20.49 ± 0.43	11.03 ± 0.89
14.92	1289370	5119	15.07	<i>g</i>	21.26 ± 0.42	6.95 ± 0.49
15.89	1373149	5119	16.03	<i>r</i>	20.83 ± 0.42	8.62 ± 0.55
15.90	1373982	10240	16.06	<i>i</i>	20.75 ± 0.42	9.25 ± 0.50
15.90	1374029	4295	16.06	<i>Y</i>	20.52 ± 0.43	11.67 ± 1.67
15.90	1374029	4295	16.06	<i>Z</i>	20.54 ± 0.43	10.73 ± 1.03
15.90	1374030	4295	16.06	<i>H</i>	20.36 ± 0.44	5.63 ± 5.26
15.90	1374030	4295	16.06	<i>J</i>	20.60 ± 0.43	8.97 ± 2.75
15.91	1374818	5119	16.05	<i>g</i>	21.29 ± 0.42	6.83 ± 0.50
16.91	1460973	4480	17.04	<i>r</i>	20.81 ± 0.42	9.13 ± 0.57
16.91	1460973	8319	17.04	<i>i</i>	20.75 ± 0.42	9.38 ± 0.52
16.91	1460979	3489	17.04	<i>Y</i>	20.55 ± 0.43	10.18 ± 2.47
16.91	1460979	3489	17.04	<i>Z</i>	20.60 ± 0.43	10.59 ± 1.12
16.91	1460981	3489	17.04	<i>J</i>	20.55 ± 0.44	8.21 ± 3.78
16.91	1461359	3839	17.02	<i>g</i>	21.33 ± 0.42	6.47 ± 0.52
17.91	1547770	3839	18.06	<i>r</i>	20.87 ± 0.42	8.51 ± 0.61
17.93	1548872	7680	18.09	<i>i</i>	20.75 ± 0.42	9.16 ± 0.55
17.93	1548882	3221	18.09	<i>Y</i>	20.59 ± 0.43	8.06 ± 2.81

Table 6
(Continued)

t_0 (day)	t_0 (s)	t_e (s)	t_f (s)	Filter	m (AB) (Aperture)	Flux (μ Jy) (PSF)
17.93	1548882	3221	18.09	Z	20.61 ± 0.43	9.09 ± 1.38
17.94	1549668	3839	18.08	g	21.39 ± 0.42	5.89 ± 0.55
18.92	1634492	6399	19.11	r	20.91 ± 0.42	7.38 ± 0.54
18.92	1634492	11359	19.11	i	20.79 ± 0.42	8.55 ± 0.50
18.92	1634525	4959	19.07	g	21.38 ± 0.42	5.56 ± 0.50
18.92	1634538	4765	19.10	J	20.48 ± 0.43	13.30 ± 2.52
18.92	1634542	4765	19.10	Y	20.57 ± 0.43	11.37 ± 1.61
18.92	1634542	4765	19.10	Z	20.59 ± 0.43	10.29 ± 0.93
19.91	1720548	6079	20.09	r	20.91 ± 0.42	7.22 ± 0.57
19.91	1720548	11120	20.09	i	20.82 ± 0.42	8.25 ± 0.52
19.91	1720583	5119	20.05	g	21.43 ± 0.42	5.28 ± 0.51
19.91	1720594	4563	20.09	J	20.59 ± 0.43	7.48 ± 2.76
19.91	1720597	4429	20.09	Y	20.57 ± 0.43	10.06 ± 2.14
19.91	1720597	4496	20.09	Z	20.70 ± 0.43	9.23 ± 1.08
20.91	1807055	6399	21.10	r	20.91 ± 0.42	7.10 ± 0.61
20.91	1807055	11439	21.10	i	20.79 ± 0.42	8.25 ± 0.56
20.92	1807079	5039	21.06	g	21.52 ± 0.43	4.36 ± 0.57
20.92	1807103	4765	21.10	J	20.78 ± 0.44	7.57 ± 3.74
20.92	1807104	4765	21.10	Z	20.58 ± 0.43	10.89 ± 1.36
20.92	1807104	4832	21.10	Y	20.60 ± 0.43	9.30 ± 2.26
21.92	1893510	6399	22.10	r	20.96 ± 0.42	6.56 ± 0.62
21.92	1893511	11519	22.10	i	20.84 ± 0.42	7.54 ± 0.57
21.92	1893520	5119	22.06	g	21.51 ± 0.43	4.19 ± 0.57
21.92	1893559	4832	22.09	J	21.04 ± 0.45	5.14 ± 3.19
21.92	1893561	4832	22.09	Z	20.59 ± 0.43	10.00 ± 1.58
21.92	1893561	4832	22.09	Y	20.64 ± 0.43	7.93 ± 2.18
22.91	1979266	5119	23.04	r	20.94 ± 0.42	6.60 ± 0.59
22.92	1980062	10240	23.07	i	20.87 ± 0.42	7.27 ± 0.51
22.93	1980833	5119	23.06	g	21.53 ± 0.43	5.10 ± 0.53
23.91	2065542	4959	24.04	g	21.46 ± 0.43	4.78 ± 0.59
23.91	2065553	6399	24.08	r	20.91 ± 0.42	6.21 ± 0.66
23.91	2065553	11519	24.08	i	20.86 ± 0.42	7.29 ± 0.54
24.99	2159267	1200	25.01	r	21.24 ± 0.44	2.72 ± 1.41
24.99	2159267	1200	25.01	i	20.92 ± 0.43	6.83 ± 1.54
25.90	2237953	4879	26.05	r	21.10 ± 0.43	5.15 ± 0.70
25.91	2238775	10000	26.08	i	20.91 ± 0.42	6.82 ± 0.58
25.91	2238821	4161	26.08	Y	20.85 ± 0.44	7.22 ± 2.92
25.91	2238821	4228	26.08	Z	20.78 ± 0.43	-0.23 ± 1.43
25.92	2239618	5039	26.07	g	21.61 ± 0.43	3.91 ± 0.67
26.91	2325407	3839	27.01	g	21.69 ± 0.43	0.00 ± 0.44
26.92	2325639	5119	27.06	r	21.07 ± 0.43	4.87 ± 0.67
26.92	2325639	8960	27.06	i	20.86 ± 0.42	7.12 ± 0.57
26.92	2325685	3758	27.06	J	20.56 ± 0.44	11.38 ± 4.12
26.92	2325688	3758	27.06	Z	20.72 ± 0.43	6.95 ± 1.48
26.92	2325688	3758	27.06	Y	20.84 ± 0.44	3.92 ± 2.48
27.90	2410506	5119	28.04	r	21.09 ± 0.43	5.85 ± 0.74
27.91	2411320	10240	28.07	i	20.96 ± 0.42	6.13 ± 0.58
27.91	2411368	4295	28.07	Z	20.84 ± 0.43	0.76 ± 1.29
27.91	2411368	4295	28.07	Y	20.86 ± 0.44	4.35 ± 2.39
27.92	2412156	5119	28.06	g	21.64 ± 0.43	3.39 ± 0.73
28.90	2496872	4959	29.04	r	21.13 ± 0.43	4.23 ± 0.63
28.91	2497696	10080	29.07	i	20.91 ± 0.42	6.33 ± 0.55
28.91	2497747	4228	29.07	Y	20.70 ± 0.43	4.82 ± 1.99
28.91	2497747	4228	29.07	Z	20.79 ± 0.43	-0.11 ± 1.18
28.92	2498536	5119	29.06	g	21.75 ± 0.43	3.35 ± 0.63
29.92	2584960	3520	30.02	r	21.15 ± 0.43	4.92 ± 0.66
29.93	2586106	7119	30.06	i	21.00 ± 0.42	5.39 ± 0.59
29.93	2586153	3020	30.06	Z	20.81 ± 0.43	-1.40 ± 1.53
29.94	2586921	3440	30.05	g	21.78 ± 0.43	2.83 ± 0.63
30.91	2670326	3199	31.00	g	21.90 ± 0.43	2.35 ± 0.63
30.91	2670536	4879	31.05	r	21.30 ± 0.43	2.88 ± 0.63
30.91	2670536	8080	31.05	i	20.97 ± 0.42	5.52 ± 0.57
30.91	2670583	3355	31.05	Y	20.66 ± 0.43	3.27 ± 2.66

Table 6
(Continued)

t_0 (day)	t_0 (s)	t_e (s)	t_f (s)	Filter	m (AB) (Aperture)	Flux (μ Jy) (PSF)
30.91	2670583	3422	31.05	Z	20.66 ± 0.43	3.83 ± 1.43
31.90	2756306	3680	32.00	<i>g</i>	21.82 ± 0.43	2.53 ± 0.53
31.90	2756574	5119	32.05	<i>r</i>	21.22 ± 0.42	2.92 ± 0.57
31.90	2756574	8800	32.05	<i>i</i>	21.00 ± 0.42	5.30 ± 0.54
31.91	2756622	3691	32.05	<i>Y</i>	20.73 ± 0.43	6.41 ± 2.60
31.91	2756622	3691	32.05	Z	20.81 ± 0.43	3.59 ± 1.38
32.90	2842792	3440	33.00	<i>g</i>	21.83 ± 0.43	2.21 ± 0.54
32.91	2843068	4879	33.05	<i>r</i>	21.22 ± 0.43	2.78 ± 0.60
32.91	2843068	8319	33.05	<i>i</i>	21.01 ± 0.42	5.33 ± 0.57
32.91	2843117	3557	33.05	Z	20.74 ± 0.43	2.95 ± 1.64
33.90	2929382	3839	34.01	<i>g</i>	21.86 ± 0.43	2.34 ± 0.48
33.91	2929674	4800	34.05	<i>r</i>	21.32 ± 0.43	2.93 ± 0.93
33.91	2929674	8960	34.05	<i>i</i>	21.02 ± 0.42	4.89 ± 0.49
34.89	3014902	3839	35.00	<i>g</i>	21.91 ± 0.43	2.23 ± 0.48
34.90	3015214	8960	35.05	<i>i</i>	21.06 ± 0.42	4.78 ± 0.50
35.90	3101699	3839	36.00	<i>g</i>	21.95 ± 0.43	1.58 ± 0.49
35.90	3101980	8960	36.05	<i>i</i>	21.06 ± 0.42	4.31 ± 0.49
35.90	3102033	2160	36.05	<i>r</i>	21.23 ± 0.44	3.30 ± 1.50
36.89	3187381	3520	37.00	<i>r</i>	21.71 ± 0.43	-0.70 ± 0.77
36.90	3188503	8080	37.04	<i>i</i>	21.08 ± 0.42	4.42 ± 0.52
38.88	3359533	3839	38.98	<i>r</i>	21.33 ± 0.43	2.55 ± 0.58
38.89	3360354	7680	39.01	<i>i</i>	21.13 ± 0.42	3.64 ± 0.53
38.89	3360403	3221	39.01	Z	20.83 ± 0.43	1.30 ± 45.53
38.90	3361179	3839	39.00	<i>g</i>	22.07 ± 0.43	1.24 ± 0.51
39.90	3446958	7680	40.01	<i>r</i>	21.34 ± 0.42	2.29 ± 0.51
39.90	3446958	7680	40.01	<i>i</i>	21.14 ± 0.42	3.80 ± 0.49
39.90	3447005	6442	40.01	H	20.73 ± 0.43	1.81 ± 2.42
39.90	3447006	6442	40.01	<i>Y</i>	20.93 ± 0.43	2.26 ± 0.94
42.92	3708410	2640	42.99	<i>i</i>	21.23 ± 0.43	4.70 ± 8.51
42.92	3708417	2214	42.99	Z	21.25 ± 0.44	0.28 ± 1.40
44.88	3877978	6399	44.98	<i>g</i>	21.98 ± 0.43	1.37 ± 0.48
44.88	3877978	6399	44.98	<i>i</i>	21.18 ± 0.42	3.12 ± 0.51
46.89	4051373	6560	47.00	<i>r</i>	21.41 ± 0.43	1.81 ± 0.56
46.89	4051373	6319	47.00	<i>i</i>	21.15 ± 0.43	2.86 ± 0.61
50.87	4395336	3680	50.93	<i>g</i>	22.11 ± 0.43	1.12 ± 0.56
50.87	4395336	3680	50.93	<i>i</i>	21.28 ± 0.43	1.64 ± 0.63
51.88	4482266	5119	51.96	<i>r</i>	21.41 ± 0.43	0.83 ± 0.56
51.88	4482267	5119	51.96	<i>i</i>	21.20 ± 0.43	2.08 ± 0.58
51.88	4482314	4295	51.96	<i>Y</i>	21.06 ± 0.43	3.62 ± 1.61
52.90	4570263	2560	52.94	<i>i</i>	21.23 ± 0.43	2.51 ± 0.74
53.88	4655540	3839	53.94	<i>r</i>	21.36 ± 0.43	2.56 ± 0.63
53.88	4655540	3839	53.94	<i>i</i>	21.16 ± 0.43	2.54 ± 0.64
53.88	4655589	3221	53.94	<i>Y</i>	21.13 ± 0.44	2.27 ± 1.56
54.88	4741565	4800	54.96	<i>g</i>	21.94 ± 0.44	1.75 ± 0.75
54.88	4741565	5119	54.96	<i>i</i>	21.29 ± 0.43	1.82 ± 0.62
54.88	4741615	2147	54.96	<i>Y</i>	20.74 ± 0.44	4.30 ± 3.39
56.88	4914230	5119	56.96	<i>r</i>	21.54 ± 0.43	-0.07 ± 1.27
56.88	4914230	5119	56.96	<i>i</i>	21.16 ± 0.43	2.96 ± 0.72
56.88	4914278	4295	56.96	<i>Y</i>	20.99 ± 0.43	1.86 ± 1.99
57.87	4999923	3839	57.93	<i>i</i>	21.40 ± 0.43	0.99 ± 0.83
58.87	5086058	3839	58.92	<i>r</i>	21.39 ± 0.43	1.18 ± 0.66
58.87	5086058	3839	58.92	<i>i</i>	21.15 ± 0.43	2.11 ± 0.68
58.87	5086106	3221	58.92	<i>Y</i>	21.03 ± 0.43	2.65 ± 1.64
59.87	5172391	3839	59.92	<i>g</i>	22.19 ± 0.43	0.50 ± 0.50
59.87	5172391	3839	59.92	<i>i</i>	21.36 ± 0.43	2.19 ± 0.61
65.86	5690438	2560	65.90	<i>i</i>	21.33 ± 0.43	1.71 ± 0.67
65.86	5690438	2560	65.90	<i>g</i>	22.20 ± 0.43	1.00 ± 0.55
66.86	5776448	2480	66.90	<i>i</i>	21.43 ± 0.43	1.61 ± 0.88
66.86	5776448	2560	66.90	<i>r</i>	21.51 ± 0.43	0.06 ± 0.79
215.15	18588991	8479	215.29	<i>r</i>	21.60 ± 0.43	0.20 ± 0.52
215.15	18588991	8479	215.29	<i>i</i>	21.35 ± 0.42	0.27 ± 0.55
217.15	18761668	8880	217.30	<i>g</i>	22.26 ± 0.43	0.10 ± 0.47
217.15	18761668	8880	217.30	<i>i</i>	21.40 ± 0.42	0.12 ± 0.52

Table 6
(Continued)

t_0 (day)	t_0 (s)	t_e (s)	t_f (s)	Filter	m (AB) (Aperture)	Flux (μJy) (PSF)
217.15	18761678	3691	217.30	Z	21.07 ± 0.43	-0.67 ± 1.20
219.14	18933938	4093	219.30	Z	21.17 ± 0.43	1.71 ± 1.18
219.14	18933983	9920	219.31	r	21.57 ± 0.42	0.12 ± 0.49
219.14	18933983	9920	219.31	i	21.41 ± 0.42	0.63 ± 0.51
221.11	19104115	6319	221.23	g	22.25 ± 0.43	0.33 ± 0.54
221.11	19104115	6560	221.23	i	21.46 ± 0.43	0.31 ± 0.79
223.14	19279069	10240	223.30	r	21.61 ± 0.42	0.27 ± 0.50
223.14	19279069	10240	223.30	i	21.45 ± 0.42	0.83 ± 0.53
223.14	19279078	4295	223.30	Z	20.99 ± 0.43	1.61 ± 1.32
229.14	19797449	4765	229.32	Z	21.06 ± 0.43	-0.32 ± 1.08
229.14	19797488	11040	229.32	g	22.26 ± 0.43	0.18 ± 0.47
229.14	19797488	11439	229.32	i	21.47 ± 0.42	0.67 ± 0.50
231.13	19969644	10479	231.33	i	21.38 ± 0.43	0.65 ± 0.61
231.13	19969803	10240	231.33	r	22.18 ± 0.43	1.05 ± 0.54
303.53	26224942	28254	384.70	Y	21.16 ± 0.43	1.31 ± 0.75
303.53	26224942	28389	384.70	Z	21.06 ± 0.43	-0.51 ± 0.59
303.53	26224983	27986	384.70	J	21.36 ± 0.43	2.10 ± 0.93
303.53	26224983	28694	384.70	H	20.86 ± 0.44	1.64 ± 1.79
306.52	26483726	79599	395.67	r	21.58 ± 0.42	0.26 ± 0.46
314.00	27129366	145272	418.10	i	21.44 ± 0.42	0.01 ± 0.45
353.44	30537092	53200	378.66	g	22.25 ± 0.42	0.10 ± 0.45
1152.86	99607079	23439	1192.87	r	21.57 ± 0.42	0.00 ± 0.44
1153.36	99650438	63920	1194.37	i	21.46 ± 0.42	-0.00 ± 0.48
1153.36	99650451	28456	1194.37	H	21.27 ± 0.44	5.55 ± 54.54
1153.36	99650451	28657	1194.37	J	21.30 ± 0.43	0.11 ± 1.62
1153.36	99650553	29463	1194.37	Y	21.34 ± 0.43	0.00 ± 0.96
1153.36	99650553	29865	1194.37	Z	21.21 ± 0.43	0.05 ± 0.73
1153.85	99692829	38160	1193.88	g	22.21 ± 0.42	0.00 ± 0.44

is $M_r = -18.43 \pm 0.11$ for SN 2013cq, which is close to the measured $M_r = -18.48 \pm 0.08$ for SN 1998bw.

5. Summary

We have presented *grizY JH* photometry of the afterglow of GRB 130427A with the RATIR instrument, from the night of the burst to three years later. Comparing our work to previous photometric studies (Xu et al. 2013a; Melandri et al. 2014; Perley et al. 2014), we have better temporal sampling, deeper photometry, and we subtract a deep late-epoch image to remove the host galaxy.

Perley et al. (2014) were better able to study the afterglow over the first couple of days and show the existence of a temporal break at about 0.7 days. Our data, on the other hand, are better suited to looking for deviations from a simple power-law model at later times associated with a supernova.

We fit the early afterglow (up to 0.7 days) and late afterglow (after 0.7 days) with power-laws. Prior to fitting for the late afterglow, we subtracted a late image to remove the contamination from the host galaxy. The temporal index of the power-law components changes from 0.97 during the early afterglow to 1.41 during the late afterglow, in agreement with the values and temporal break around 0.7 days determined by Maselli et al. (2014) and Perley et al. (2014).

Positive residuals to the fits in *griz* between about 7 and 40 days show that we are seeing the photometric signature of SN 2013cq, previously detected spectroscopically by de Ugarte Postigo et al. (2013) and Xu et al. (2013a) and photometrically by Perley et al. (2014), Xu et al. (2013a), and Melandri et al.

(2014). The absolute magnitude and broadband SED of the supernova are consistent with those of the prototype SN 1998bw and suggest similar progenitors. The peak times agree with those reported by Xu et al. (2013a) and are detailed for *griz* bands. The absolute magnitudes calculated match with SN 1998bw for *riz* bands. Our better temporal coverage and deeper photometry give us an improved light curve compared to previous work (Xu et al. 2013a; Melandri et al. 2014; Perley et al. 2014). Photometric data obtained three years after the GRB 130427A suggest that the host galaxy is extremely blue compared to local samples.

GRB 130427A is among the handful of events with a confirmed GRB/SN association. In addition it is a high-luminosity event, differing from sub-luminous, very local ones such as GRB 980425/SN 1998bw. The combination is thus unique, and the detailed, homogeneous photometry are presented here with the aim of enlarging the sample for which detailed inferences can be made, eventually in a more statistically significant way when combined with other bursts.

We thank the staff of the Observatorio Astronómico Nacional in Sierra San Pedro Mártil. We thank the anonymous referee for a very helpful report. We thank Fabio De Colle for useful comments on earlier drafts. RATIR is a collaboration between the University of California, the Universidad Nacional Autónoma de México, NASA Goddard Space Flight Center, and Arizona State University, benefiting from the loan of an H2RG detector and hardware and software support from Teledyne Scientific and Imaging. RATIR, the automation of the Harold L.

Table 7
Residuals between Observations and the Power-law Model for RATIR Data for Early Afterglow (Before 0.7 days)

t_0 (s)	Filter				
	i (μ Jy)	Z (μ Jy)	Y (μ Jy)	J (μ Jy)	H (μ Jy)
929	1099.93 \pm 539.14
1009	...	2805.23 \pm 601.42
1012	3354.17 \pm 649.69	...
1037	1373.25 \pm 518.59
1111	591.10 \pm 605.02
1114	2951.70 \pm 651.46
1140	314.13 \pm 467.87
1216	-497.04 \pm 535.12	...	2238.44 \pm 567.07
1249	-34.68 \pm 385.64
1323	...	832.70 \pm 441.93
1326	1761.38 \pm 465.51	...
1348	-541.16 \pm 341.65
1429	705.36 \pm 425.84	...
1432	...	207.34 \pm 388.42
1457	-341.40 \pm 325.81
1532	271.86 \pm 473.29
1534	398.85 \pm 421.20
1579	-344.62 \pm 303.13
1653	760.35 \pm 424.83	...	413.36 \pm 387.92
1683	-10.17 \pm 294.07
1762	...	237.31 \pm 321.87
1764	362.12 \pm 345.01	...
1778	-26.80 \pm 276.89
1858	702.49 \pm 330.55	...
1859	...	98.84 \pm 303.47
1887	-345.25 \pm 280.13
1962	260.62 \pm 336.24
1964	843.22 \pm 386.70
1993	63.20 \pm 253.56
2067	116.67 \pm 309.69
2068	810.12 \pm 362.53
2120	-776.28 \pm 223.10
2196	...	1021.73 \pm 282.60	...	-721.88 \pm 256.29	...
2223	-304.10 \pm 218.44
2298	416.47 \pm 272.67	...
2300	...	-45.74 \pm 248.32
2328	11.83 \pm 217.43
2408	365.80 \pm 287.64	...	-10.21 \pm 276.78
2422	-416.26 \pm 212.59
2502	-192.37 \pm 258.31
2506	191.98 \pm 266.82
2531	-446.33 \pm 184.76
2605	26.02 \pm 236.63	...
2607	...	-175.13 \pm 217.63
2654	-305.91 \pm 178.58
2729	-206.29 \pm 217.49	...
2732	...	-567.47 \pm 204.66
2780	-522.44 \pm 193.74
2855	-77.25 \pm 243.18
2856	106.19 \pm 273.15
2884	-204.39 \pm 164.74
2960	-147.92 \pm 218.22
2961	605.39 \pm 291.40
2990	-278.80 \pm 162.89
3067	...	-239.20 \pm 178.90
3069	-166.34 \pm 196.09	...
3108	-360.19 \pm 150.44
3186	...	77.07 \pm 182.57	...	-1002.49 \pm 167.46	...
3213	-362.91 \pm 150.66
3292	-227.89 \pm 191.97
3293	329.50 \pm 284.11
3307	-333.22 \pm 144.97
3387	247.13 \pm 256.03
3389	-131.45 \pm 190.18
3418	-168.13 \pm 156.71
3493	...	-169.05 \pm 185.52	...	-868.70 \pm 156.80	...
3535	-105.29 \pm 140.17
3610	...	-128.75 \pm 158.66
3611	-100.35 \pm 168.94	...
3640	-217.72 \pm 133.67

Table 7
(Continued)

t_0 (s)	Filter				
	i (μ Jy)	Z (μ Jy)	Y (μ Jy)	J (μ Jy)	H (μ Jy)
3719	491.39 ± 228.38
3721	11.29 ± 175.04
3735	-143.56 ± 143.25
3814	-144.77 ± 170.13
3815	476.88 ± 207.06
3842	-116.80 ± 128.28
3918	-245.69 ± 183.08	...
3919	...	-282.94 ± 158.48
3963	-22.03 ± 123.97
4038	...	429.42 ± 154.41	...	-334.68 ± 144.00	...
4069	-204.18 ± 131.80
4145	294.22 ± 210.48
4146	88.92 ± 159.62
4171	-43.37 ± 129.77
4247	403.42 ± 206.94
4248	92.01 ± 155.91
4295	-68.97 ± 114.90
4371	...	430.77 ± 141.70	...	-268.65 ± 134.35	...
4414	20.95 ± 113.41
4493	...	405.50 ± 142.94	...	-305.07 ± 129.43	...
4523	-753.30 ± 142.08
4598	-62.47 ± 384.04	...	-379.43 ± 186.04
4642	128.93 ± 111.30
4718	68.32 ± 145.11
4719	193.53 ± 181.91
4742	13.53 ± 106.79
4821	-34.60 ± 133.02	...
4822	...	-10.51 ± 122.19
4846	3.86 ± 107.35
4922	16.76 ± 130.56	...
4923	...	-1574.14 ± 86.59
4953	12.21 ± 106.93
5028	826.11 ± 322.54
5032	216.10 ± 150.56
5059	33.37 ± 106.53
5134	422.64 ± 177.33
5135	270.93 ± 131.95
5186	-59.76 ± 133.88
5260	107.47 ± 126.22	...
5262	...	139.56 ± 115.97
5287	187.44 ± 103.88
5362	...	402.54 ± 128.18	...	-101.23 ± 111.83	...
5394	48.19 ± 97.91
5470	732.22 ± 209.78	...	207.25 ± 125.30
5506	22.50 ± 97.93
5586	605.06 ± 160.57	...	124.24 ± 126.73
5615	165.21 ± 94.75
5690	255.73 ± 118.96	...
5694	...	-29.63 ± 109.85
5715	176.93 ± 92.38
5789	338.34 ± 120.32	...
5790	...	224.85 ± 106.05
5823	203.43 ± 90.44
5897	557.04 ± 129.97
5898	112.54 ± 123.03
5942	-57.18 ± 99.26
6018	240.91 ± 114.64
6020	782.68 ± 182.53
6050	120.56 ± 87.90
6124	236.29 ± 108.81	...
6125	...	138.35 ± 99.38

Table 8
Residuals between Observations and the Power-law Model for RATIR Data for Late Afterglow (After 0.7 days)

t_0 (day)	Filter						
	g (μ Jy)	r (μ Jy)	i (μ Jy)	Z (μ Jy)	Y (μ Jy)	J (μ Jy)	H (μ Jy)
0.83	...	-23.90 ± 3.62	-37.66 ± 3.51	-48.43 ± 9.07	-50.50 ± 9.44	-66.74 ± 10.87	-54.80 ± 10.22
0.85	...	-20.88 ± 4.07	-38.87 ± 3.49	-46.55 ± 9.88	-31.91 ± 10.33	-56.30 ± 9.97	-46.25 ± 17.28
0.87	...	-21.47 ± 2.53	-25.19 ± 3.31	-41.10 ± 7.91	-40.88 ± 9.58	-29.30 ± 9.93	-41.91 ± 9.72
0.90	...	-15.79 ± 4.17	-32.39 ± 3.86	-39.28 ± 8.21	-56.57 ± 7.43	-39.85 ± 8.11	-50.19 ± 7.82
0.92	...	-22.70 ± 2.79	-28.13 ± 3.29	-40.63 ± 7.88	-26.98 ± 7.88	-69.72 ± 7.39	-14.33 ± 8.76
0.94	...	-19.90 ± 2.81	-32.23 ± 3.14	-35.16 ± 5.39	-37.45 ± 8.05	-30.91 ± 8.56	14.00 ± 8.31
0.97	...	-14.07 ± 3.22	-24.73 ± 3.38	-26.06 ± 6.43	-28.58 ± 7.58	-35.32 ± 7.58	-7.64 ± 7.58
0.99	...	-12.95 ± 3.62	-25.80 ± 2.90	-22.56 ± 7.51	-42.19 ± 6.59	-38.27 ± 7.29	10.01 ± 7.96
1.01	...	-7.59 ± 3.37	-26.91 ± 3.13	-21.96 ± 7.38	-30.36 ± 7.26	-21.45 ± 7.40	-17.75 ± 7.80
1.04	...	-10.58 ± 3.01	-20.13 ± 3.02	-18.67 ± 9.83	-30.09 ± 7.18	-22.21 ± 8.67	-25.60 ± 10.30
1.06	...	-15.91 ± 3.58	-19.59 ± 3.08	-40.60 ± 8.52	-25.47 ± 7.58	-16.84 ± 9.29	-5.48 ± 10.43
1.83	...	-1.14 ± 1.17	-2.56 ± 1.76	3.03 ± 4.45	6.59 ± 4.86	-8.12 ± 7.28	10.77 ± 8.73
1.85	...	-2.12 ± 1.08	-2.66 ± 1.67	-5.28 ± 3.94	5.02 ± 5.26	-3.83 ± 6.66	0.36 ± 8.23
1.87	...	-1.21 ± 1.19	-1.91 ± 1.62	-7.42 ± 4.18	4.85 ± 5.26	-7.31 ± 6.44	12.60 ± 8.85
1.89	...	0.36 ± 0.86	-2.55 ± 1.24	-0.80 ± 3.64	1.51 ± 4.21	-9.33 ± 5.33	21.06 ± 7.82
1.91	...	-2.19 ± 1.04	-2.26 ± 1.60	-1.96 ± 3.56	3.04 ± 4.33	-4.08 ± 5.43	3.01 ± 6.82
1.93	...	-1.24 ± 1.32	-2.41 ± 1.59	-0.62 ± 3.54	0.67 ± 4.26	-3.65 ± 5.17	16.87 ± 7.51
1.96	...	0.51 ± 1.52	-1.73 ± 1.48	2.56 ± 3.65	4.93 ± 4.65	-3.31 ± 7.80	19.87 ± 6.70
1.98	...	-1.38 ± 1.62	-0.24 ± 1.41	-5.77 ± 3.98	13.89 ± 4.77	1.87 ± 5.53	43.92 ± 10.52
2.00	...	-2.54 ± 1.24	1.08 ± 1.59	6.36 ± 4.22	-3.77 ± 4.65	-5.57 ± 5.55	35.66 ± 7.94
2.02	...	-2.07 ± 1.33	0.57 ± 1.47	5.51 ± 6.66	10.72 ± 9.75
2.03	3.21 ± 4.22	-3.50 ± 5.05
2.04	...	-0.80 ± 1.60	-1.18 ± 1.93	5.76 ± 7.21	31.37 ± 11.22
2.83	...	0.04 ± 0.68	-1.22 ± 1.01	5.82 ± 2.89	13.99 ± 4.88	-3.86 ± 6.33	22.36 ± 8.99
2.85	...	1.91 ± 1.01	0.51 ± 1.14	-0.35 ± 3.12	10.05 ± 4.87	2.82 ± 7.44	5.39 ± 11.54
2.87	...	2.22 ± 0.70	0.25 ± 0.99	3.65 ± 2.81	17.59 ± 5.00	-1.42 ± 5.62	19.63 ± 8.72
2.89	...	1.50 ± 0.81	0.05 ± 0.88	5.80 ± 2.37	-2.79 ± 3.37	-6.73 ± 4.70	6.42 ± 6.93
2.91	...	0.41 ± 0.78	-0.30 ± 0.93	-2.00 ± 2.60	2.25 ± 3.87	-1.02 ± 4.80	9.47 ± 7.36
2.93	...	0.20 ± 0.96	-0.41 ± 0.94	-0.22 ± 2.62	2.15 ± 5.01	2.52 ± 4.73	23.24 ± 7.61
2.95	...	0.07 ± 0.97	-0.34 ± 0.97	4.08 ± 2.62	10.02 ± 4.21	6.05 ± 4.63	14.62 ± 7.89
2.97	...	-0.39 ± 0.81	-0.72 ± 0.98	-0.90 ± 2.91	5.18 ± 4.19	-0.48 ± 4.68	32.10 ± 8.50
2.99	...	0.64 ± 0.94	2.30 ± 1.04	-2.29 ± 2.99	9.74 ± 4.75	2.42 ± 5.21	8.66 ± 9.56
3.02	...	-2.13 ± 0.81	3.50 ± 1.16	0.04 ± 2.88	9.46 ± 4.54	6.81 ± 5.12	20.49 ± 9.20
3.04	...	2.05 ± 1.00	-0.43 ± 1.02	0.30 ± 3.10	4.02 ± 4.53	0.98 ± 5.47	21.31 ± 9.52
3.82	...	-0.42 ± 0.82	0.05 ± 0.87
3.84	...	1.05 ± 0.72	1.35 ± 0.80
3.86	...	1.65 ± 0.67	0.46 ± 0.69
3.88	...	0.38 ± 0.63	0.40 ± 0.76
3.90	...	0.15 ± 0.75	-0.69 ± 0.74
3.92	...	1.34 ± 0.67	0.73 ± 0.80
3.94	...	0.52 ± 0.76	0.61 ± 0.75
3.96	...	0.13 ± 0.62	0.59 ± 0.68
3.97	...	1.37 ± 0.69	2.55 ± 0.82
4.00	...	0.42 ± 0.65	0.31 ± 0.66
4.01	...	2.02 ± 0.71	2.76 ± 0.75
4.03	...	0.88 ± 0.75	0.02 ± 0.86
5.03	-1.51 ± 0.81	-2.30 ± 0.95	1.03 ± 0.84
5.94	...	1.83 ± 0.33
5.95	1.78 ± 0.35	0.08 ± 0.90	1.67 ± 1.29	7.04 ± 1.60	3.14 ± 2.62
5.97	-0.46 ± 0.24
6.93	0.53 ± 0.22	...	1.75 ± 0.33	3.24 ± 0.89	1.94 ± 1.35	8.00 ± 2.36	0.91 ± 2.76
7.94	0.45 ± 0.26	...	1.42 ± 0.35
7.95	2.07 ± 1.01	5.42 ± 1.54	10.57 ± 2.09	24.92 ± 3.36
9.96	0.51 ± 0.23	...	2.37 ± 0.36	3.07 ± 1.16	3.25 ± 1.72	2.34 ± 2.31	-20.23 ± 3.90
10.91	...	2.27 ± 0.90
10.93	0.22 ± 0.62	...	2.48 ± 0.38	0.63 ± 1.11	3.45 ± 1.77	9.80 ± 2.97	...
11.93	1.31 ± 0.23	2.76 ± 0.29	2.69 ± 0.23	2.05 ± 0.67	1.99 ± 1.01	-0.66 ± 1.35	3.62 ± 2.13
12.91	1.68 ± 0.23	3.14 ± 0.31	3.28 ± 0.26	3.37 ± 0.76	4.80 ± 1.19	5.42 ± 1.69	-10.94 ± 2.49
13.91	1.77 ± 0.21	3.02 ± 0.32	2.67 ± 0.24	1.70 ± 0.73	3.44 ± 1.17	8.17 ± 1.60	-11.87 ± 2.51
14.90	...	3.59 ± 0.30
14.91	3.15 ± 0.23	2.43 ± 0.67	4.01 ± 1.01	6.37 ± 1.39	5.74 ± 2.11
14.92	1.89 ± 0.21
15.89	...	3.18 ± 0.33

Table 8
(Continued)

t_0 (day)	Filter						
	g (μ Jy)	r (μ Jy)	i (μ Jy)	Z (μ Jy)	Y (μ Jy)	J (μ Jy)	H (μ Jy)
15.90	2.86 ± 0.25	2.86 ± 0.77	2.85 ± 1.14	0.35 ± 1.55	-4.27 ± 2.23
15.91	2.21 ± 0.25
16.91	2.23 ± 0.28	4.15 ± 0.36	3.52 ± 0.28	3.38 ± 0.82	2.10 ± 1.45	0.30 ± 1.85	...
17.91	...	3.91 ± 0.41
17.93	3.77 ± 0.33	2.45 ± 0.97	0.61 ± 1.57
17.94	1.98 ± 0.34
18.92	1.94 ± 0.25	3.12 ± 0.31	3.55 ± 0.25	4.14 ± 0.70	4.46 ± 1.12	6.55 ± 1.47	...
19.91	1.91 ± 0.26	3.26 ± 0.37	3.60 ± 0.28	3.51 ± 0.80	3.64 ± 1.34	1.20 ± 1.55	...
20.91	...	3.40 ± 0.42	3.91 ± 0.34
20.92	1.21 ± 0.36	5.55 ± 0.96	3.31 ± 1.38	1.71 ± 1.84	...
21.92	1.24 ± 0.37	3.10 ± 0.42	3.47 ± 0.37	5.00 ± 1.11	2.32 ± 1.35	-0.34 ± 1.68	...
22.91	...	3.35 ± 0.39
22.92	3.45 ± 0.27
22.93	2.34 ± 0.30
23.91	2.17 ± 0.39	3.15 ± 0.47	3.69 ± 0.31
24.99	...	-0.16 ± 1.02	3.45 ± 1.08
25.90	...	2.42 ± 0.51
25.91	3.61 ± 0.38	-4.18 ± 1.03	2.79 ± 1.60
25.92	1.59 ± 0.48
26.91	-2.20 ± 0.00
26.92	...	2.28 ± 0.48	4.08 ± 0.36	3.20 ± 1.06	-0.28 ± 1.46	7.28 ± 1.94	...
27.90	...	3.38 ± 0.55
27.91	3.24 ± 0.37	-2.79 ± 0.92	0.36 ± 1.43
27.92	1.29 ± 0.54
28.90	...	1.89 ± 0.44
28.91	3.58 ± 0.33	-3.49 ± 0.86	1.02 ± 1.28
28.92	1.35 ± 0.43
29.92	...	2.69 ± 0.47
29.93	2.77 ± 0.39	-4.62 ± 1.08
29.94	0.93 ± 0.43
30.91	0.54 ± 0.44	0.75 ± 0.44	3.01 ± 0.36	0.75 ± 0.99	-0.19 ± 1.52
31.90	0.80 ± 0.30	0.88 ± 0.36	2.91 ± 0.32
31.91	0.64 ± 1.01	3.11 ± 1.50
32.90	0.55 ± 0.33
32.91	...	0.83 ± 0.40	3.04 ± 0.37	0.13 ± 1.13
33.90	0.75 ± 0.21
33.91	...	1.06 ± 0.70	2.70 ± 0.23
34.89	0.70 ± 0.21
34.90	2.67 ± 0.24
35.90	0.11 ± 0.22	1.57 ± 1.07	2.28 ± 0.22
36.89	...	-2.36 ± 0.58
36.90	2.47 ± 0.28
38.88	...	1.01 ± 0.37
38.89	1.83 ± 0.31	-0.93 ± 6.74
38.90	-0.07 ± 0.26
39.90	...	0.80 ± 0.27	2.06 ± 0.23	...	-0.16 ± 0.71	...	-0.89 ± 1.43
42.92	3.12 ± 2.86	-1.66 ± 1.02
44.88	0.29 ± 0.19	...	1.64 ± 0.27
46.89	...	0.62 ± 0.35	1.47 ± 0.41
50.87	0.22 ± 0.34	...	0.40 ± 0.43
51.88	...	-0.20 ± 0.34	0.88 ± 0.38	...	1.95 ± 1.12
52.90	1.34 ± 0.55
53.88	...	1.59 ± 0.44	1.40 ± 0.45	...	0.69 ± 1.10
54.88	0.94 ± 0.56	...	0.70 ± 0.43	...	2.76 ± 1.74
56.88	...	-0.97 ± 0.91	1.91 ± 0.53	...	0.39 ± 1.28
57.87	-0.04 ± 0.63
58.87	...	0.32 ± 0.47	1.10 ± 0.49	...	1.26 ± 1.13
59.87	-0.21 ± 0.25	...	1.20 ± 0.42
65.86	0.38 ± 0.34	...	0.85 ± 0.49
66.86	...	-0.66 ± 0.59	0.77 ± 0.66
215.15	...	0.06 ± 0.29	0.11 ± 0.33
217.15	-0.02 ± 0.19	...	-0.04 ± 0.28	-0.87 ± 0.87
219.14	...	-0.02 ± 0.23	0.47 ± 0.26	1.51 ± 0.86

Table 8
(Continued)

t_0 (day)	Filter						
	g (μ Jy)	r (μ Jy)	i (μ Jy)	Z (μ Jy)	Y (μ Jy)	J (μ Jy)	H (μ Jy)
221.11	0.21 ± 0.32	...	0.16 ± 0.59
223.14	...	0.13 ± 0.25	0.67 ± 0.30	1.42 ± 0.94
229.14	0.07 ± 0.17	...	0.53 ± 0.25	-0.50 ± 0.80
231.13	...	0.92 ± 0.31	0.51 ± 0.41
303.53	-0.64 ± 0.39	1.17 ± 0.56	1.96 ± 0.70	1.49 ± 1.20
306.52	...	0.18 ± 0.15
314.00	-0.09 ± 0.09
353.44	0.04 ± 0.09
1152.86	...	-0.01 ± 0.00
1153.36	-0.02 ± 0.19	0.03 ± 0.54	-0.02 ± 0.72	0.09 ± 1.12	5.53 ± 7.37
1153.85	-0.01 ± 0.00

Johnson Telescope of the Observatorio Astronómico Nacional in Sierra San Pedro Mártir, and the operation of both are funded through NASA grants NNX09AH71G, NNX09AT02G, NNX10AI27G, and NNX12AE66G, CONACyT grants INFR-2009-01-122785 and CB-2008-101958, UNAM PAPIIT grants IG100414 and IA102917, UC MEXUS-CONACyT grant CN 09-283, and the Instituto de Astronomía of the Universidad Nacional Autónoma de México.

References

- Ackermann, M., Ajello, M., Asano, K., et al. 2014, *Sci*, **343**, 42
- Barthelmy, S. D., Baumgartner, W. H., Cummings, J. R., et al. 2013, GCN, **14470**, 1
- Becker, A. 2015, HOTPANTS: High Order Transform of PSF ANd Template Subtraction, Astrophysics Source Code Library, ascl:[1504.004](#)
- Berger, E., Chornock, R., Holmes, T. R., et al. 2011, *ApJ*, **743**, 204
- Berger, E., Fox, D. B., Cucchiara, A., & Cenko, S. B. 2008, GCN, **8335**, 1
- Bersier, D. 2012, arXiv:[1206.6979](#)
- Bloom, J. S., Kulkarni, S. R., Price, P. A., et al. 2002, *ApJL*, **572**, L45
- Bufano, F., Pian, E., Sollerman, J., et al. 2012, *ApJ*, **753**, 67
- Butler, N., Klein, C., Fox, O., et al. 2012, *Proc. SPIE*, **8446**, 844610
- Campana, S., Mangano, V., Blustin, A. J., et al. 2006, *Natur*, **442**, 1008
- Cano, Z., Bersier, D., Guidorzi, C., et al. 2011, *ApJ*, **740**, 41
- Cano, Z., de Ugarte Postigo, A., Perley, D., et al. 2015, *MNRAS*, **452**, 1535
- Chornock, R., Berger, E., Levesque, E. M., et al. 2010, arXiv:[1004.2262](#)
- Clocchiatti, A., Suntzeff, N. B., Covarrubias, R., & Candia, P. 2011, *AJ*, **141**, 163
- Cobb, B. E., Bloom, J. S., Perley, D. A., et al. 2010, *ApJL*, **718**, L150
- D'Elia, V., Pian, E., Melandri, A., et al. 2015, *A&A*, **577**, A116
- de Ugarte Postigo, A., Xu, D., Leloudas, G., et al. 2013, GCN, **14646**, 1
- Della Valle, M., Benetti, S., Mazzali, P., et al. 2008, CBET, **1602**, 1
- Della Valle, M., Malesani, D., Benetti, S., et al. 2003, *A&A*, **406**, L33
- Della Valle, M., Malesani, D., Bloom, J. S., et al. 2006, *ApJL*, **642**, L103
- Eichler, D., Livio, M., Piran, T., & Schramm, D. N. 1989, *Natur*, **340**, 126
- Ferrero, P., Kann, D. A., Zeh, A., et al. 2006, *A&A*, **457**, 857
- Flores, H., Covino, S., Xu, D., et al. 2013, GCN, **14491**, 1
- Foley, S., Watson, D., Gorosabel, J., et al. 2006, *A&A*, **447**, 891
- Fox, O. D., Kutyrev, A. S., Rapchun, D. A., et al. 2012, *Proc. SPIE*, **8453**, 845310
- Fraija, N. 2015, *ApJ*, **804**, 105
- Fraija, N., Lee, W., & Veres, P. 2016, *ApJ*, **818**, 190
- Fraija, N., Lee, W., Veres, P., & Barniol Duran, R. 2016, *ApJ*, **831**, 22
- Fruchter, A. S., Levan, A. J., Strolger, L., et al. 2006, *Natur*, **441**, 463
- Fynbo, J. U., Holland, S., Andersen, M. I., et al. 2000, *ApJL*, **542**, L89
- Galama, T. J., Vreeswijk, P. M., van Paradijs, J., et al. 1998, *Natur*, **395**, 670
- Gal-Yam, A., Moon, D.-S., Fox, D. B., et al. 2004, *ApJL*, **609**, L59
- Garnavich, P. M., Stanek, K. Z., Wyrszynowski, L., et al. 2003, *ApJ*, **582**, 924
- Gavazzi, G., Fumagalli, M., Cucciati, O., & Boselli, A. 2010, *A&A*, **517**, A73
- Greiner, J., Klose, S., Reinsch, K., et al. 2003, *Natur*, **426**, 157
- Hammer, F., Flores, H., Schaerer, D., et al. 2006, *A&A*, **454**, 103
- Hjorth, J. 2013, *RSPTA*, **371**, 20120275
- Hjorth, J., & Bloom, J. S. 2012, in Gamma-Ray Bursts, ed. C. Kouveliotou, R. A. M. J. Wijers, & S. Woosley (Cambridge: Cambridge Univ. Press)
- Koshut, T. M., Paciesas, W. S., Kouveliotou, C., et al. 1995, *BAAS*, **27**, 53.01
- Kouveliotou, C., Meegan, C. A., Fishman, G. J., et al. 1993, *ApJL*, **413**, L101
- Kumar, P., & Piran, T. 2000, *ApJ*, **532**, 286
- Kumar, P., & Zhang, B. 2015, *PhR*, **561**, 1
- Lang, D., Hogg, D. W., Mierle, K., Blanton, M., & Roweis, S. 2010, *AJ*, **139**, 1782
- Lattimer, J. M., & Schramm, D. N. 1976, *ApJ*, **210**, 549
- Lee, W. H., & Ramirez-Ruiz, E. 2007, *NJPh*, **9**, 17
- Levan, A. J., Cenko, S. B., Perley, D. A., & Tanvir, N. R. 2013, GCN, **14455**, 1
- Levan, A. J., Tanvir, N. R., Fruchter, A. S., et al. 2014, *ApJ*, **792**, 115
- Littlejohns, O. M., Butler, N. R., Cucchiara, A., et al. 2015, *MNRAS*, **449**, 2919
- MacFadyen, A. I., & Woosley, S. E. 1999, *ApJ*, **524**, 262
- Malesani, D., Tagliaferri, G., Chincarini, G., et al. 2004, *ApJL*, **609**, L5
- Maselli, A., Melandri, A., Nava, L., et al. 2014, *Sci*, **343**, 48
- Matheson, T., Garnavich, P. M., Stanek, K. Z., et al. 2003, *ApJ*, **599**, 394
- Melandri, A., Pian, E., D'Elia, V., et al. 2014, *A&A*, **567**, A29
- Melandri, A., Pian, E., Ferrero, P., et al. 2012, *A&A*, **547**, A82
- Mirabal, N., Halpern, J. P., An, D., Thorstensen, J. R., & Terndrup, D. M. 2006, *ApJL*, **643**, L99
- Modjaz, M. 2011, *AN*, **332**, 434
- Modjaz, M., Kewley, L., Kirshner, R. P., et al. 2008, *AJ*, **135**, 1136
- Nakar, E. 2007, *PhR*, **442**, 166
- Narayan, R., Paczynski, B., & Piran, T. 1992, *ApJL*, **395**, L83
- Niino, Y. 2013, in EAS Publications Ser. 61 Gamma-ray Bursts: 15 Years of GRB Afterglows, ed. A. J. Castro-Tirado et al. (Les Ulis: EDP Sciences), 427
- Olivares, E. F., Greiner, J., Schady, P., et al. 2012, *A&A*, **539**, A76
- Paczynski, B. 1989, *ApJL*, **308**, L43
- Paczynski, B. 1991, *AcA*, **41**, 257
- Perley, D. A., Cenko, S. B., Corsi, A., et al. 2014, *ApJ*, **781**, 37
- Pian, E., Mazzali, P. A., Masetti, N., et al. 2006, *Natur*, **442**, 1011
- Planck Collaboration, Ade, P. A. R., Aghanim, N., et al. 2014, *A&A*, **571**, A1
- Sari, R., & Piran, T. 1998
- Sari, R., & Piran, T. 1999, *ApJ*, **520**, 641
- Schulze, S., Malesani, D., Cucchiara, A., et al. 2014, *A&A*, **566**, A102
- Soderberg, A., Berger, E., & Fox, D. N. 2008, GCN, **8662**, 1
- Stanek, K. Z., Matheson, T., Garnavich, P. M., et al. 2003, *ApJL*, **591**, L17
- Starling, R. L. C., Wiersema, K., Levan, A. J., et al. 2011, *MNRAS*, **411**, 2792
- Tam, P.-H. T., Tang, Q.-W., Hou, S.-J., Liu, R.-Y., & Wang, X.-Y. 2013, *ApJL*, **771**, L13
- Thomsen, B., Hjorth, J., Watson, D., et al. 2004, *A&A*, **419**, L21
- Tinney, C., Stathakis, R., Cannon, R., et al. 1998, IAUC, **6896**, 1
- Toy, V. L., Cenko, S. B., Silverman, J. M., et al. 2015, arXiv:[1508.00575](#)
- Vestrand, W. T., Wren, J. A., Panaiteescu, A., et al. 2014, *Sci*, **343**, 38
- Vonova, A., Elenin, L., & Pozanenko, A. 2013, GCN, **14516**, 1
- von Kienlin, A. 2013, GCN, **14473**, 1
- Watson, A. M., Butler, N., Kutyrev, A., et al. 2013, GCN, **14666**, 1
- Watson, A. M., Richer, M. G., Bloom, J. S., et al. 2012, *Proc. SPIE*, **8444**, 84445L
- Woosley, S. E. 1993, *ApJ*, **405**, 273
- Woosley, S. E., & Bloom, J. S. 2006, *ARA&A*, **44**, 507
- Xu, D., de Ugarte Postigo, A., Leloudas, G., et al. 2013a, *ApJ*, **776**, 98
- Xu, D., de Ugarte Postigo, A., Schulze, S., et al. 2013b, GCN, **14478**, 1



Erratum: “Photometric Observations of Supernova 2013cq Associated with GRB 130427A (2017, APJ, 837, 116)”

R. L. Becerra¹, A. M. Watson¹, W. H. Lee¹, N. Fraija¹, N. R. Butler², J. S. Bloom³, J. I. Capone⁴, A. Cucchiara⁵, J. A. de Diego¹, O. D. Fox⁶, N. Gehrels⁷, L. N. Georgiev¹, J. J. González¹, A. S. Kutyrev⁷, O. M. Littlejohns², J. X. Prochaska⁸, E. Ramirez-Ruiz⁸, M. G. Richer⁹, C. G. Román-Zúñiga⁹, V. L. Toy⁴, and E. Troja^{4,7}

¹ Instituto de Astronomía, Universidad Nacional Autónoma de México, Apartado Postal 70-264, 04510 México, D. F., México

² School of Earth and Space Exploration, Arizona State University, Tempe, AZ 85287, USA

³ Department of Astronomy, University of California, Berkeley, CA 94720-3411, USA

⁴ Department of Astronomy, University of Maryland, College Park, MD 20742, USA

⁵ NASA Postdoctoral Program Fellow, Goddard Space Flight Center, Greenbelt, MD 20771, USA

⁶ Space Telescope Science Institute, 3700 San Martin Drive, Baltimore, MD 21218, USA

⁷ NASA, Goddard Space Flight Center, Greenbelt, MD 20771, USA

⁸ Department of Astronomy and Astrophysics, UCO/Lick Observatory, University of California, 1156 High Street, Santa Cruz, CA 95064, USA

⁹ Instituto de Astronomía, Universidad Nacional Autónoma de México, Apartado Postal 106, 22800 Ensenada, Baja California, México

Received 2017 May 17; published 2017 June 14

Supporting material: machine-readable table

Appendix

- (1) In of Table 6, t_f is stated as being in seconds, but the values are actually in days.
- (2) There is an error in our code to generate Table 6 that caused the column with the uncertainties in the aperture photometry to be incorrect. This error has no effect on the other columns in the table, on the figures, or on our analysis.

Table 6
 Photometry of GRB 130427A

t_0 (d)	t_0 (s)	t_e (s)	t_f (d)	Filter	m (AB)	Flux (μJy) (PSF)
0.01	930	80	0.01	<i>i</i>	12.88 ± 0.02	
0.01	1009	67	0.01	Z	12.75 ± 0.02	
0.01	1012	67	0.01	J	12.69 ± 0.02	
0.01	1037	80	0.01	<i>i</i>	12.97 ± 0.02	
0.01	1111	67	0.01	H	12.86 ± 0.02	
0.01	1114	67	0.01	Y	12.77 ± 0.02	
0.01	1141	80	0.01	<i>i</i>	13.12 ± 0.02	
0.01	1216	67	0.01	Y	12.88 ± 0.02	
0.01	1216	67	0.01	H	13.00 ± 0.02	
0.01	1249	80	0.02	<i>i</i>	13.24 ± 0.02	

Note. Table 6 is published in its entirety in the electronic edition of the *Astrophysical Journal*. A portion is shown here for guidance regarding its form and content.

(This table is available in its entirety in machine-readable form.)